IEEE Access
Multidisciplinary ⋮ Rapid Review ⋮ Open Access Journal

Received 28 September 2023, accepted 6 November 2023, date of publication 8 November 2023,
date of current version 15 November 2023.

Digital Object Identifier 10.1109/ACCESS.2023.3331575

RESEARCH ARTICLE

RIS-Aided Mixed RF-FSO Wireless Networks: Secrecy Performance Analysis With Simultaneous Eavesdropping

MD. MIJANUR RAHMAN[1], A. S. M. BADRUDDUZA[1], (Member, IEEE), NOOR AHMAD SARKER[1], MD. IBRAHIM[2], (Graduate Student Member, IEEE), IMRAN SHAFIQUE ANSARI[3], (Senior Member, IEEE), AND HEEJUNG YU[4], (Senior Member, IEEE)

[1]Department of Electronics and Telecommunication Engineering, Rajshahi University of Engineering and Technology (RUET), Rajshahi 6204, Bangladesh
[2]Institute of ICT, Rajshahi University of Engineering and Technology (RUET), Rajshahi 6204, Bangladesh
[3]James Watt School of Engineering, University of Glasgow, G12 8QQ Glasgow, U.K.
[4]Department of Electronics and Information Engineering, Korea University, Sejong 30019, South Korea

Corresponding author: Heejung Yu (heejungyu@korea.ac.kr)

This work was supported in part by the "Regional Innovation Strategy (RIS)" through the National Research Foundation of Korea (NRF) funded by the Ministry of Education (MOE) under Grant 2021RIS-004; in part by the Basic Science Research Program through NRF funded by MOE under Grant 2021R1I1A3041887; in part by the Ministry of Science and ICT (MIST), South Korea, through the Information Technology Research Center (ITRC) Support Program, supervised by the Institute for Information and Communications Technology Planning and Evaluation (IITP), under Grant IITP-2023-RS-2022-00164800; and in part by the Korea University Grant.

ABSTRACT In order to meet the demands of diverse services within sixth-generation networks across a range of industries, numerous approaches are being employed to address notable signal degradation resulting from channel obstruction, particularly in the realms of millimeter wave and sub-THz frequencies. One of these solutions is the utilization of reconfigurable intelligent surfaces (RISs), which can reflect or refract signals in the desired direction. This integration offers significant potential to improve the coverage area from a transmitter to a receiver. In this paper, we present a comprehensive framework for analyzing the secrecy performance of an RIS-aided mixed radio frequency (RF)-free space optics (FSO) system employing in terms of physical layer security (PLS). It is assumed that a secure message is transmitted from a RF transmitter to a FSO receiver through an intermediate relay. The RF link experiences Rician fading while the FSO link experiences Málaga distributed turbulence with pointing errors. Three different eavesdropping scenarios are examined: 1) RF-link eavesdropping, 2) FSO-link eavesdropping, and 3) simultaneous eavesdropping attack on both RF and FSO links. We evaluate the secrecy performance using analytical expressions to compute secrecy metrics such as the average secrecy capacity, secrecy outage probability, probability of strictly positive secrecy capacity, effective secrecy throughput, and intercept probability. Our results are confirmed via Monte-Carlo simulations and demonstrate that fading parameters, atmospheric turbulence conditions, pointing errors, and detection techniques play a crucial role in enhancing secrecy performance.

INDEX TERMS Physical layer security, reconfigurable intelligent surface, Rician fading, Málaga fading, pointing error.

I. INTRODUCTION

A. BACKGROUND AND LITERATURE STUDY

As the beyond fifth generation (B5G) and sixth generation (6G) of wireless communication have emerged, reconfigurable intelligent surfaces (RISs) to address the negative impacts of wireless channels have been explored as one of the most crucial technologies [1], [2], [3], [4], [5]. To create a truly intelligent environment, there is a significant strategy to control the wireless medium, i.e., signal reflection direction, in an intentional way [6]. To address this need, an RIS has been developed using passive components that can be programmed and managed through an RIS controller allowing it to reflect signals toward specific directions

The associate editor coordinating the review of this manuscript and approving it for publication was Angelo Trotta.

as required [7]. Furthermore, the mixed radio frequency (RF)-free space optical (FSO) systems are considered potential structures for the next-generation wireless networks [8]. The use of RISs in both RF and FSO transmissions can help solve signal blockage issues that arise in wireless communication channels.

FSO communications are seen as a promising option that can provide fast data transmission speeds and be applied in a range of scenarios such as serving as a backup to fiber, supporting wireless networks for backhauling, and aiding in disaster recovery efforts [9]. However, they are vulnerable to pointing errors and atmospheric conditions and are not suitable for transmitting information over long distances. Through the implementation of relaying strategy, the dual-hop RF-FSO mixed models merge the strengths of RF and FSO communication technologies [10], [11]. In [12], the authors demonstrated how pointing errors, atmospheric turbulence, and path loss affect a mixed FSO-RF system and provided insights for improving the design and operation of such systems. The authors of [13] derived analytical expressions for the outage probability (OP), average data rate, and ergodic capacity (EC) of the RF-FSO systems, and assessed the performance in the presence of multiple users with various data rate requirements. Recently, the authors of [14], [15], [16], and [17] enhanced the dual-hop performance by optimizing the system parameters and made it suitable for space-air-ground integrated networks.

There has been a lot of research in the literature where single RIS-aided systems have been investigated [18], [19], [20], [21], [22], [23], [24]. In [18], the accuracy and effectiveness of RIS-assisted systems in modifying wireless signals were evaluated by assuming practical factors such as phase shift and amplitude response that can affect their performance. In [19], it was demonstrated that RISs could improve system performance over a Nakagami-m fading channel by examining signal-to-noise ratio (SNR) and channel capacity. The findings of the study also provide insights into how to optimize RIS-empowered communications in practical scenarios. The system performance of an RIS-aided network is assessed by the authors of [20] wherein they suggested that the number of reflecting elements used in the network does not affect the diversity gain. On the other hand, the system performance of an RIS-aided dual-hop network was analyzed in [25], [26], [27], [28], and [29]. For example, the authors of [25] conducted a study comparing RIS-equipped RF sources and RIS-aided RF sources, and suggested that mixed RF-FSO relay networks utilizing these two types of sources offer great potential for enhancing the performance of wireless communication networks in various environments, both indoors and outdoors. In [26], it was concluded that incorporating RIS in mixed FSO-RF systems can greatly enhance the coverage area. This is achieved by improving the signal quality and reducing the signal attenuation that may occur during transmission. However, it was observed that RISs can help mitigate the impact of interference from nearby channels in dual-hop communication systems with co-channel interference [27]. The authors of [28] proposed a study on the effect of different system parameters, including the number and placement of RIS elements, on the performance of an RIS-assisted communication system. Here, the authors concluded that the most effective RIS configuration for optimal performance depends on the specific communication scenario and network requirements. In [30], a RIS-assisted FSO-RF mixed model with hybrid automatic repeat request techniques was proposed where the OP and packet error rate was derived in closed form to evaluate the system performance.

Wireless communications face a significant challenge in terms of protecting the privacy of information because their inherent characteristics make them vulnerable to security threats [31]. Till date, the security of wireless communication has relied on different encryption and decryption techniques that take place in the higher levels of the protocol stack [32]. Newly suggested physical layer security (PLS) methods are now seen as a practical solution to stop unauthorized eavesdropping in wireless networks by utilizing the unpredictable nature of time-varying wireless channels [33], [34], [35], [36], [37], [38]. Recently, extensive research has been conducted to explore the secrecy performance of mixed RF-FSO systems. The authors of [39] concluded that using a mixed model offers better security compared to using RF or FSO technology alone, and they emphasized the importance of implementing appropriate security measures and techniques. Another study in [40] examined the secrecy performance of a mixed RF-FSO relay channel with variable gain while [41] provided insights into the secrecy performance of a cooperative relaying system and emphasized the significance of selecting suitable statistical models and security techniques. In [42], the authors examined the trade-off between security and reliability in a DF-based FSO-RF system, demonstrating that employing receiver diversity leads to improved secrecy performance. The reference [43] presents an analysis of the secrecy performance in a scenario where an RF backhaul system is augmented with a parallel FSO communication link to enhance data transmission security. In [44], the authors demonstrated a mixed FSO-RF cooperative system that takes simultaneous eavesdropping into account. Their findings revealed that a low pointing error and heterodyne detection (HD) at the receiver results in improved performance. Additionally, the authors in [45] evaluated the performance of the mixed RF-FSO system with a wireless-powered friendly jammer and analyzed the impact of different system parameters on secrecy performance. On the other hand, some challenges and limitations associated with the dual-hop model were identified in [46] including the impact of atmospheric turbulence on the FSO link's performance and the importance of accurate channel estimation. Finally, a new model for the mixed RF-FSO channel was presented in [47] that takes into account arbitrary correlation, and the results showed that both correlation and pointing error could significantly affect the secure outage performance of the model. Although

a lot of research has looked into the investigation of PLS analysis due to the RF-FSO mixed systems [39], [40], [41], [42], [43], [44], [45], [46], [47], the potential of RIS to improve confidentiality in wireless networks has not been extensively studied in the context of RIS-assisted RF-FSO systems. It is worth noting that recent research has explored the RIS-aided model, even in the context of the single hop only, which significantly differs from our proposed system. Many of these studies have focused on utilizing Rayleigh distributions [6], [48] and Nakagami-*m* distributions [49] to assess secrecy performance. However, there are also studies such as [50] that have investigated the PLS of a non-orthogonal multiple access (NOMA)-based visible light communication-RF mixed system where the authors looked into the influence of RIS on secrecy performance. Furthermore, a different perspective was taken in [51], where the authors analyzed a high-altitude platform-based RF-FSO model. In this case, they considered Nakagami-*m* and Rayleigh distributions for the RF link, and they assumed a Gamma-Gamma distribution for the FSO link.

B. MOTIVATION AND CONTRIBUTIONS

Although RIS-aided mixed RF-FSO systems are strong contenders for upcoming B5G and 6G wireless networks and their diverse applications, there has been limited investigation into their capacity to maintain secrecy in the available literature. The current literature mainly focuses on mixed RF-FSO systems and does not fully investigate the security performance of RIS-assisted RF-FSO systems from a perspective of physical layer security (PLS) particularly when RIS is used in both links [52]. In this paper, we conduct a PLS analysis of the RIS-aided RF-FSO system configuration and evaluate its secrecy performance under the simultaneous influence of RF and FSO eavesdropping attacks, which, to the best of the authors' knowledge, has not been inspected before for this type of configuration. In addition, since wireless channels experience frequent variation over time, assuming a Rician channel in the RF links would provide a more realistic environment to model the wireless propagation perfectly [53]. Meanwhile, the Málaga fading distribution applied to the FSO link in the system being examined produces reliable results, particularly in challenging atmospheric turbulence and pointing error scenarios [47]. Motivated by these advantages, we introduce a secure wireless network over the Rician-Málaga mixed RF-FSO fading channel model. The key contributions of this research are as follows:

- In the past few decades, numerous studies have investigated the secrecy performance of mixed RF-FSO systems, such as [39], [40], [41], [45], [46], [47], [54], and [55]. However, the secrecy performance of dual-hop systems that incorporate both RF and FSO links aided by RISs remains an open concept, with no research conducted on this specific configuration up to date. In this paper, we propose an RIS-aided mixed RF-FSO network in the presence of two different eavesdroppers accounting for their ability to intercept information transmitted through both RF and FSO links. It is important to highlight that while there has been a recent investigation into the secrecy performance of the RIS-assisted model [6], [48], [49], [50], [51], their studies are significantly different from our proposed structure in terms of both the system model and the statistical characteristics being considered.
- Firstly, we obtain the cumulative distribution function (CDF) of the dual-hop RF-FSO system under decode-and-forward (DF) relaying protocols by utilizing the CDF of each link. Furthermore, we develop the new analytical expressions of average secrecy capacity (ASC), the lower bound of secrecy outage probability (SOP), the probability of strictly positive secrecy capacity (SPSC), effective secrecy throughput (EST), and intercept probability (IP). These expressions are novel compared to the previous works because the proposed model is completely different from the existing RF-FSO literature.
- The derived expressions are utilized to obtain numerical results with specific configurations. Furthermore, we confirm the precision of the analytical results through Monte-Carlo (MC) simulations. This validation through simulation strengthens the reliability of our analysis.
- In an effort to increase the practicality of our analysis, we provide insightful remarks that shed light on the design of secure RIS-aided mixed RF-FSO relay networks. To ensure a more realistic analysis, we take into account the major impairments and features of both RF and FSO links. For instance, we incorporate the impacts of fading parameters and the number of reflecting elements for RF links, as well as atmospheric turbulence, detection techniques, and pointing error conditions for FSO links.

C. ORGANIZATION

The paper is organized into several sections. Section II provides an introduction to the models of the system and channel that are utilized in the study. In Section III, the paper presents analytical expressions for five significant performance metrics including ASC, SOP, and the probabilities of SPSC, EST, and IP. Section IV provides enlightening discussions and numerous numerical examples. Finally, Section V serves as the conclusion to the paper.

II. SYSTEM MODEL AND PROBLEM FORMULATION

As depicted in Fig. 1, we present the system model of a RIS-aided combined RF-FSO DF-based relaying system where a RIS-RF system forms the first hop and the second hop is composed of a RIS-FSO system. Since a source, denoted by $\mathcal{S}$ (ground control station, smartphone, etc), and a relay, denoted by $\mathcal{R}$ (tall building), cannot communicate directly due to obstructions, $\mathcal{S}$ link to $\mathcal{R}$ through a RIS, denoted $\mathcal{I}_P$, mounted on a structure. Similarly, communication between $\mathcal{R}$ and a destination, denoted

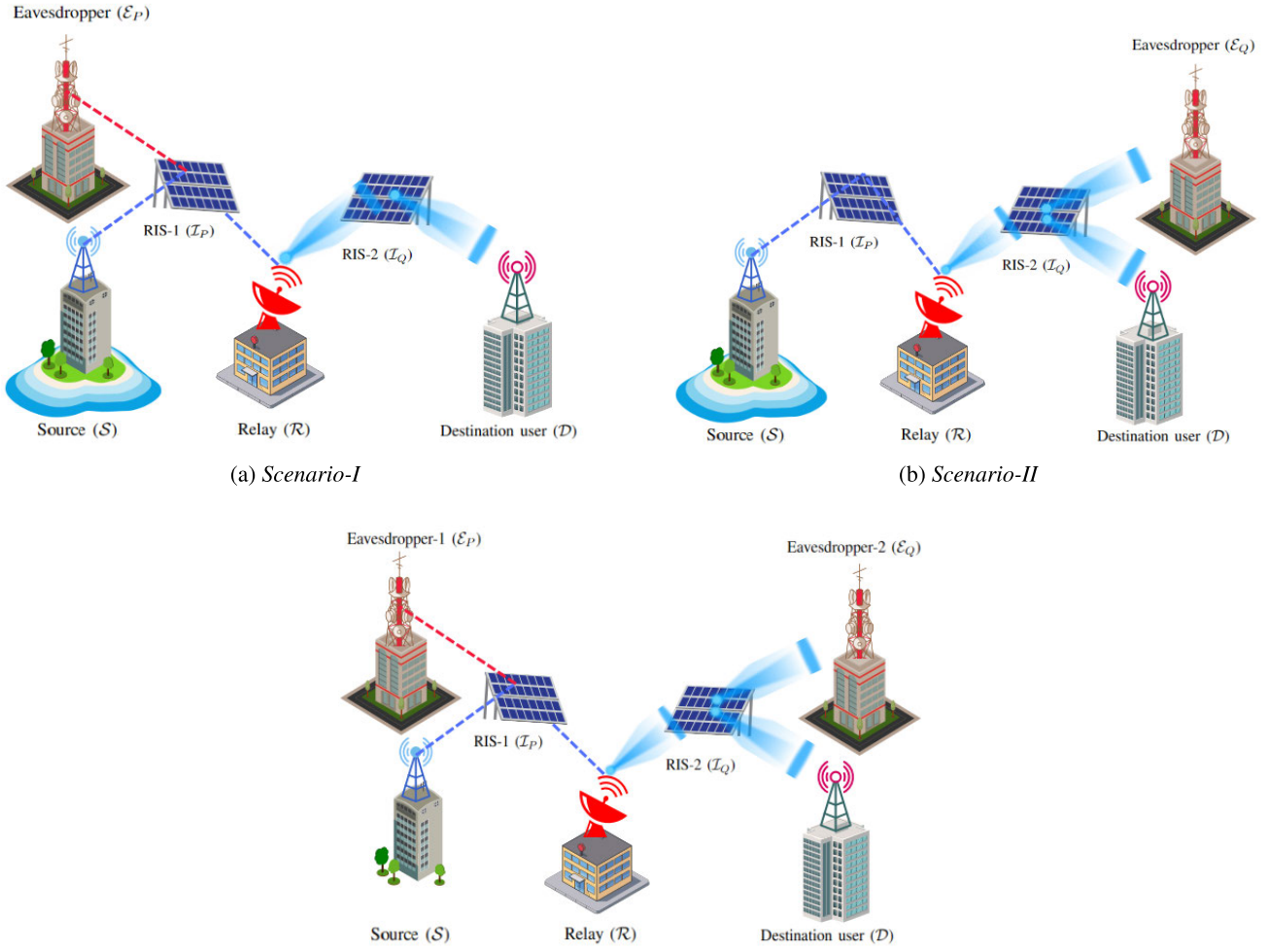

(a) *Scenario-I* (b) *Scenario-II*

(c) *Scenario-III*

FIGURE 1. System model of a combined RIS-aided dual-hop RF-FSO system with source ($\mathcal{S}$), relay ($\mathcal{R}$), the destination user ($\mathcal{D}$), and eavesdroppers ($\mathcal{E}_P$ and $\mathcal{E}_Q$).

by $\mathcal{D}$ (satellite ground station, smartphones, drone, etc), is established through another RIS, i.e., $\mathcal{I}_Q$). A RIS works as an intermediate medium between $\mathcal{S}$ and $\mathcal{R}$ with a view to ensuring a line-of-sight path between two nodes. In practical applications, RF-FSO mixed systems offer versatile solutions to address specific communication challenges and enhance performance. The mixed models find use in industrial sensor networks, aerial surveillance drones, secure military communication, hybrid data centers, and internet-of-things (IoT)-enabled smart buildings, showcasing the adaptability and benefits of combining RF and FSO technologies to meet diverse communication needs. The unauthorized users, which are known as eavesdroppers, denoted by $\mathcal{E}$ (smartphone, drone, etc), attempt to intercept the confidential information that is transmitted from $\mathcal{S}$ to $\mathcal{D}$. Based on the position of eavesdroppers, three different scenarios are considered where the eavesdropper attempts to overhear the communication between $\mathcal{S}$ and $\mathcal{D}$ via $\mathcal{R}$.

- In *Scenario-I* (Fig. 1a), the eavesdropper, $\mathcal{E}_P$, utilizes the RF link for wiretapping and both $\mathcal{R}$ and $\mathcal{E}_P$ attain analogous signal propagated from $\mathcal{I}_P$.
- The *Scenario-II* (Fig. 1b) infers the eavesdropper, $\mathcal{E}_Q$, at the FSO link and both $\mathcal{D}$ and $\mathcal{E}_Q$ obtain the resembling propagated signal from $\mathcal{I}_Q$.
- In *Scenario-III* (Fig. 1c), the eavesdroppers $\mathcal{E}_P$ and $\mathcal{E}_Q$ both attempt concurrently to overhear the confidential information from both the RF and FSO links.

This model describes a passive eavesdropping scenario assuming that the RIS is oblivious to the CSI of eavesdroppers. Herein, $\mathcal{S}$ and $\mathcal{E}$ are equipped with a singular antenna, while $\mathcal{R}$ acts as a transceiver. $\mathcal{D}$ comprises a single photo-detector for optical wave reception, while $\mathcal{I}_P$ and $\mathcal{I}_Q$ have $\mathcal{N}_1$ and $\mathcal{N}_2$ reflecting elements, respectively. The surface RF networks using $\mathcal{S}-\mathcal{I}_P-\mathcal{R}$ and $\mathcal{S}-\mathcal{I}_P-\mathcal{E}_P$ links pursue the Rician fading distribution. $\mathcal{R}$ serves to convert the obtained RF signal and redirect it as optical signal to $\mathcal{D}$ in the presence of $\mathcal{E}_Q$. Both the FSO links, $\mathcal{R}-\mathcal{I}_Q-\mathcal{D}$ and $\mathcal{R}-\mathcal{I}_Q-\mathcal{E}_Q$ experience Málaga turbulence with pointing error aided by an RIS, $\mathcal{I}_Q$.

A. SNRS OF INDIVIDUAL LINKS

For *Scenario-I*, h_{s_p} ($s_p = 1, 2, \ldots, \mathcal{N}_1$) indicates the first hop channel gain between $\mathcal{S}$ and $\mathcal{I}_P$ in both $\mathcal{S} - \mathcal{I}_P - \mathcal{R}$ and $\mathcal{S} - \mathcal{I}_P - \mathcal{E}_P$ links. Similarly, g_{s_p} and n_{s_p} indicate the channel gains of the second hop from $\mathcal{I}_P$ to $\mathcal{R}$ and $\mathcal{E}_P$, respectively. Hence, the signals at $\mathcal{R}$ and $\mathcal{E}_P$ are expressed by

$$y_{s,r} = \left[\sum_{s_p=1}^{\mathcal{N}_1} h_{s_p} e^{j\Phi_{s_p}} g_{s_p}\right] x + w_1, \tag{1}$$

$$y_{s,e} = \left[\sum_{s_p=1}^{\mathcal{N}_1} h_{s_p} e^{j\Psi_{s_p}} n_{s_p}\right] x + w_2, \tag{2}$$

respectively. For the channels of each particular link, we have

$$h_{s_p} = \alpha_{s_p} e^{j\varrho_{s_p}}$$
$$g_{s_p} = \beta_{s_p} e^{j\vartheta_{s_p}}$$
$$n_{s_p} = \eta_{s_p} e^{j\delta_{s_p}}$$

where α_{s_p}, β_{s_p}, and η_{s_p} are the Rician distributed random variables (RVs), ϱ_{s_p}, ϑ_{s_p}, and δ_{s_p} are the resembling phases of received signal gains. Moveover, Φ_{s_p} and Ψ_{s_p} identifies the phases emanated by the s_p-th reflecting element of the RIS. In this work, we consider $\Phi_{s_p} \in [0, 2\pi)$, $\Psi_{s_p} \in [0, 2\pi)$, and the range of reflection on the assembled fortuitous signal present at the s_p-th element is deliberated as 1. The conveyed data from $\mathcal{S}$ is represented in this scenario by x with the power S_s and $w_1 \sim \widetilde{\mathcal{M}}(0, M_r)$, $w_2 \sim \widetilde{\mathcal{M}}(0, M_e)$ are the additive white Gaussian noise (AWGN) samples with M_r, M_e indicating the power of noise for the relevant networks. Mathematically, (1) and (2) are expressed as

$$y_{s,r} = g^T \Phi\, h\, x + w_1, \tag{3}$$

$$y_{s,e} = n^T \Psi\, h\, x + w_2, \tag{4}$$

where the channel coefficient vectors are denoted by

$$h = [h_1\, h_2\, \ldots\, h_{\mathcal{N}_1}]^T,$$
$$g = [g_1\, g_2\, \ldots\, g_{\mathcal{N}_1}]^T,$$
$$n = [n_1\, n_2\, \ldots\, n_{\mathcal{N}_1}]^T,$$
$$\Phi = \text{diag}([e^{j\Phi_1}\, e^{j\Phi_2}\, \ldots\, e^{j\Phi_{\mathcal{N}_1}}]),$$
$$\Psi = \text{diag}([e^{j\Psi_1}\, e^{j\Psi_2}\, \ldots\, e^{j\Psi_{\mathcal{N}_1}}]).$$

Φ and Ψ are the diagonal matrices containing the transitions of phase employed by RIS components. The SNRs at $\mathcal{R}$ and $\mathcal{E}_P$ are expressed as

$$\gamma_r = \left[\sum_{s_p=0}^{\mathcal{N}_1} \alpha_{s_p}\beta_{s_p} e^{j\left(\Phi_{s_p} - \varrho_{s_p} - \vartheta_{s_p}\right)}\right]^2 \bar{\gamma}_r, \tag{5}$$

$$\gamma_{e_p} = \left[\sum_{s_p=0}^{\mathcal{N}_1} \alpha_{s_p}\eta_{s_p} e^{j\left(\Psi_{s_p} - \varrho_{s_p} - \delta_{s_p}\right)}\right]^2 \bar{\gamma}_{e_p}, \tag{6}$$

where the average SNR of the $\mathcal{S} - \mathcal{I}_P - \mathcal{R}$ link is denoted by $\bar{\gamma}_r = \frac{S_s}{M_r}$ and the average SNR of $\mathcal{S} - \mathcal{I}_P - \mathcal{E}_P$ link is represented by $\bar{\gamma}_{e_p} = \frac{S_s}{M_e}$. Therefore, the ideal selection of Φ_{s_p} and Ψ_{s_p} are $\Phi_{s_p} = \varrho_{s_p} + \vartheta_{s_p}$ and $\Psi_{s_p} = \varrho_{s_p} + \delta_{s_p}$ for obtaining maximized instantaneous SNRs. It is worth noting that similar to the research conducted by [56] and [57], we make the assumption of the most adverse eavesdropping scenario, where the eavesdropper possesses strong detection capabilities. Hence, the maximum possible SNRs at $\mathcal{R}$ and $\mathcal{E}_P$ are given, correspondingly, as

$$\gamma_r = \left(\sum_{s_p=0}^{\mathcal{N}_1} \alpha_{s_p}\beta_{s_p}\right)^2 \bar{\gamma}_r, \tag{7}$$

$$\gamma_{e_p} = \left(\sum_{s_p=0}^{\mathcal{N}_1} \alpha_{s_p}\eta_{s_p}\right)^2 \bar{\gamma}_{e_p}. \tag{8}$$

For *Scenario-II*, the received signals at $\mathcal{D}$ and $\mathcal{E}_Q$ are represented in a form similar to the expressions in (1)-(4) and utilizing the same procedures for optimization, the received SNRs are given as

$$\gamma_d = \left(\sum_{r_q=0}^{\mathcal{N}_2} \xi_{r_q}\beta_{r_q}\right)^2 \bar{\gamma}_d, \tag{9}$$

$$\gamma_{e_q} = \left(\sum_{r_q=0}^{\mathcal{N}_2} \xi_{r_q}\eta_{r_q}\right)^2 \bar{\gamma}_{e_q}, \tag{10}$$

where ξ_{r_q}, β_{r_q}, and η_{r_q} are Málaga distributed RVs, $\bar{\gamma}_d$ and $\bar{\gamma}_{e_q}$ are the average SNRs of the $\mathcal{R}-\mathcal{I}_Q-\mathcal{D}$ and $\mathcal{R}-\mathcal{I}_Q-\mathcal{E}_Q$ links, respectively. The received SNR at the destination utilizing a DF relay is given by

$$\gamma_{eq} \cong \min\{\gamma_r, \gamma_d\}. \tag{11}$$

B. PDF AND CDF OF RIS-AIDED RF LINKS

The probability density function (PDF) and CDF of γ_j, where $j \in (r, e_p)$ are respectively expressed as [53]

$$f_{\gamma_j}(\gamma) \simeq \frac{\gamma^{\frac{a_j-1}{2}} \exp\left(-\frac{\sqrt{\gamma}}{b_j\sqrt{\bar{\gamma}_j}}\right)}{2b_j^{a_j+1}\Gamma(a_j+1)\bar{\gamma}_j^{\frac{a_j+1}{2}}}, \tag{12}$$

$$F_{\gamma_j}(\gamma) \simeq \frac{\gamma\left(a_j+1, \frac{\sqrt{\gamma}}{b_j\sqrt{\bar{\gamma}_j}}\right)}{\Gamma(a_j+1)}, \tag{13}$$

where $\gamma(\cdot,\cdot)$ is the lower incomplete Gamma function [58, Eq. (8.350.1)], $\Gamma(\cdot)$ is the Gamma operator, a_j and b_j are constants related to the mean and variance of the cascaded Rician random variable ξ_j computed as

$$a_j = \frac{\mathbb{E}^2[\xi_j]}{\text{Var}(\delta_j)} - 1, \tag{14}$$

$$b_j = \frac{\text{Var}(\delta_j)}{\mathbb{E}[\xi_j]}, \tag{15}$$

where ξ_m is the sum of i.i.d. non-negative random variables,

$$\mathbb{E}\left[\xi_j\right] = \mathbb{E}\left[\alpha_{sp}\right]\mathbb{E}\left[\lambda_{sp}\right], \tag{16}$$

$\lambda \in (\beta, \eta)$ and $\mathbb{E}\left[\alpha_{sp}\right] = \frac{1}{2}\sqrt{\frac{\pi\Omega_1}{K_1+1}}L_{1/2}\left(-K_1\right)$, $\mathbb{E}\left[\lambda_{sp}\right] = \frac{1}{2}\sqrt{\frac{\pi\Omega_j}{K_j+1}}L_{1/2}\left(-K_j\right)$, $\mathrm{Var}(\delta_j) = \mathcal{N}_1\mathrm{Var}\left(\xi_j\right)$, K_1 and Ω_1 denote the shape parameter and scale parameter, respectively, for the first hop of $\mathcal{S} - \mathcal{I}_P - \mathcal{R}$ link, for the other hop those are expressed by K_j and Ω_j, correspondingly, $L_{1/2}(\cdot)$ denotes the Laguerre polynomial, i.e., $L_{1/2}(x) = e^{x/2}\left[(1-x)I_0\left(\frac{-x}{2}\right) - xI_1\left(\frac{-x}{2}\right)\right]$, and $I_v(\cdot)$ is the modified Bessel function of the first kind and order v [58, Eq. (8.431)]. Further simplification of (16) gives

$$\begin{aligned}\mathbb{E}\left[\xi_j\right] = {} & \frac{\pi e^{-\frac{(K_1+K_j)}{2}}}{4}\sqrt{\frac{\Omega_1\Omega_j}{(K_1+1)\left(K_j+1\right)}} \\ & \times\left[(K_1+1)\,I_0\left(\frac{K_1}{2}\right) + K_1 I_1\left(\frac{K_1}{2}\right)\right] \\ & \times\left[\left(K_j+1\right)I_0\left(\frac{K_j}{2}\right) + K_j I_1\left(\frac{K_j}{2}\right)\right].\end{aligned} \tag{17}$$

Notice that $\mathbb{E}\left[\xi_j^2\right] = \mathbb{E}\left[\alpha_{sp}^2\right]\mathbb{E}\left[\lambda_{sp}^2\right] = \Omega_1\Omega_j$. The variance is computed as

$$\mathrm{Var}\left(\delta_j\right) = \mathbb{E}\left[\xi_j^2\right] - \mathbb{E}^2\left[\xi_j\right] = \Omega_1\Omega_j - \mathbb{E}^2\left[\xi_j\right]. \tag{18}$$

C. PDF AND CDF OF RIS-AIDED FSO LINKS

The PDF of γ_p, where $p \in (d, e_q)$, can be calculated as [59, Eq. (17)]

$$f_{\gamma_p}(\gamma) = \int_0^\infty f_{\gamma_h}(t) f_{\gamma_{gp}}\left(\frac{\gamma}{t}\right)\frac{1}{t}dt. \tag{19}$$

The PDFs of $\mathcal{R}-\mathcal{I}_Q$, $\mathcal{I}_Q-\mathcal{D}$ and $\mathcal{I}_Q-\mathcal{E}_Q$ links can be written as [60, Eq. (10)]

$$f_{\gamma_i}(\gamma_i) = \frac{\xi_i^2 A_i}{2^r\gamma_i}\sum_{m_i=1}^{\beta_i} b_{m_i} \mathrm{G}_{1,3}^{3,0}\left[B_i\left(\frac{\gamma_i}{\bar{\gamma}_i}\right)^{\frac{1}{r}}\middle|\begin{matrix}\xi_i^2+1 \\ \xi_i^2, \alpha_i, m_i\end{matrix}\right], \tag{20}$$

where $i \in \{h, g_p\}$,

$$\begin{aligned} A_i &\triangleq \frac{2{\alpha_i}^{\alpha_i/2}}{c^{1+\alpha_i/2}\Gamma(\alpha_i)}\left(\frac{c\beta_i}{c\beta_i+\Omega'}\right)^{\beta_i+\alpha_i/2}, \\ a_{m_i} &\triangleq \binom{\beta_i-1}{m_i-1}\frac{\left(c\beta_i+\Omega'\right)^{1-m_i/2}}{(m_i-1)!}\left(\frac{\Omega'}{c}\right)^{m_i-1}\left(\frac{\alpha_i}{\beta_i}\right)^{\frac{m_i}{2}}, \\ b_{mi} &= a_{mi}[\alpha_i\beta_i/(c\beta_i+\Omega')]^{-(\alpha_i+m_i)/2}, \\ B_i &= \xi_i^2\alpha_i\beta_i(c+\Omega' t)/[(\xi_i^2+1)(c\beta_i+\Omega')], \\ \Omega' &= \Omega + 2b_0\rho + 2\sqrt{2b_0\rho\Omega}\cos(\phi_A-\phi_B), \end{aligned}$$

and $c = 2b_0(1-\rho)$ indicates the average amount of power received by off-axis eddies from the dispersive element, α_i and β_i are the turbulence parameters, $\bar{\gamma}_i$ is the average SNR, ξ_i represents pointing error, Ω is the average power of LOS component, b_0 is the average power of the total scatter components, ρ represents the quantity of scattering power coupled to the LOS component, ϕ_A and ϕ_B are the deterministic phases of the LOS and the coupled-to-LOS scatter terms, respectively, $r \in \{1, 2\}$ determines if the transmission makes use of the heterodyne detection (HD) approach ($r = 1$) or the intensity modulation/direct detection (IM/DD) techniques ($r = 2$) [60], and $\mathbf{G}_{p,q}^{m,n}\left[z \mid \begin{matrix}a_p \\ b_q\end{matrix}\right]$ is the Meijer's G function [58, Eq. (9.301)]. From (20), we get

$$f_{\gamma_h}(t) = \frac{\xi_h^2 A_h}{2^r t}\sum_{m_h=1}^{\beta_h} b_{m_h} G_{1,3}^{3,0}\left[B_h\left(\frac{t}{\bar{\gamma}_h}\right)^{\frac{1}{r}}\middle|\begin{matrix}{\xi_h}^2+1 \\ {\xi_h}^2, \alpha_h, m_h\end{matrix}\right], \tag{21}$$

$$\begin{aligned} f_{\gamma_{gp}}\left(\frac{\gamma}{t}\right) = {} & \frac{\xi_{g_p}^2 A_{g_p} t}{2^r\gamma}\sum_{m_{gp}=1}^{\beta_{gp}} b_{m_{gp}} \\ & \times G_{1,3}^{3,0}\left[B_{g_p}\left(\frac{\gamma}{t\bar{\gamma}_{g_p}}\right)^{\frac{1}{r}}\middle|\begin{matrix}{\xi_{g_p}}^2+1 \\ {\xi_{g_p}}^2, \alpha_{g_p}, m_{g_p}\end{matrix}\right], \end{aligned} \tag{22}$$

where $\bar{\gamma}_h$ and $\bar{\gamma}_{g_p}$ are the average SNRs. In (22), the variable t appears in the denominator. Utilizing the Meijer's G function's reflection characteristic [61] in (22), we get

$$\begin{aligned} & f_{\gamma_{gp}}\left(\frac{\gamma}{t}\right) \\ & = \frac{\xi_{g_p}^2 A_{g_p} t}{2^r\gamma}\sum_{m_{gp}=1}^{\beta_g} b_{m_{gp}} \\ & \quad \times G_{3,1}^{0,3}\left[\frac{1}{B_{g_p}}\left(\frac{t\bar{\gamma}_{g_p}}{\gamma}\right)^{\frac{1}{r}}\middle|\begin{matrix}1-{\xi_{g_p}}^2, 1-\alpha_{g_p}, 1-m_{g_p} \\ -\xi_{g_p}^2\end{matrix}\right]. \end{aligned} \tag{23}$$

Substituting (21) and (23) into (19) then applying the change of variable $X = t^{\frac{1}{a}} \Rightarrow t = X^a$ and $dt = aX^{a-1}dX$ via utilizing [62, Eq. (2.24.1.1)], we obtain the exact unified PDF of end-to-end SNR as

$$\begin{aligned} & f_{\gamma_p}(\gamma) \\ & = \frac{\xi_h^2 A_h \xi_{g_p}^2 A_{g_p} r}{2^{2r}\gamma}\sum_{m_h=1}^{\beta_h}\sum_{m_{gp}=1}^{\beta_{gp}} b_{m_h} b_{m_{gp}} \\ & \quad \times G_{2,6}^{6,0}\left[B_h B_{g_p}\left(\frac{\gamma}{\bar{\gamma}_p}\right)^{\frac{1}{r}}\middle|\begin{matrix}1+{\xi_{g_p}}^2, 1+\xi_h^2 \\ {\xi_h}^2, \alpha_h, m_h, \xi_{g_p}^2, \alpha_{g_p}, m_{g_p}\end{matrix}\right], \end{aligned} \tag{24}$$

where $\bar{\gamma}_p = \bar{\gamma}_h\bar{\gamma}_{g_p}$. The CDF of the end-to-end SNR can be written as

$$F_{\gamma_p}(\gamma) = \int_0^\gamma f_{\gamma_p}(\gamma)d\gamma. \tag{25}$$

By substituting (24) into (25), we obtain the CDF of γ_p via utilizing [63, Eq. (07.34.21.0084.01)] as

$$F_{\gamma_p}(\gamma)=\frac{\xi_h^2 A_h \xi_{g_p}^2 A_{g_p}}{2^{2r}} \sum_{m_h=1}^{\beta_h} \sum_{m_{g_p}=1}^{\beta_{g_p}} b_{m_h} b_{m_{g_p}} \frac{r^{\alpha_h+\alpha_{g_p}+m_h+m_{g_p}-2}}{2\pi^{2(r-1)}} \times G_{2r+1,6r+1}^{6r,1}\left[\left(\frac{B_{hg_p}}{\bar{\gamma}_p}\right)\gamma \middle| \begin{matrix} 1, l_{g_{p_1}}, l_{h_1} \\ l_{h_2}, l_{g_{p_2}}, 0 \end{matrix}\right], \quad (26)$$

where

$$B_{hg_p} = \frac{\left(B_h B_{g_p}\right)^r}{r^{4r}},$$
$$l_{g_{p_1}} = \left(\frac{1+{\xi_{g_p}}^2}{r}, \ldots, \frac{1+{\xi_{g_p}}^2+r-1}{r}\right),$$
$$l_{h_1} = \left(\frac{1+{\xi_h}^2}{r}, \ldots, \frac{1+{\xi_h}^2+r-1}{r}\right),$$
$$l_{g_{p_2}} = \left(\frac{{\xi_{g_p}}^2}{r}, \ldots, \frac{{\xi_{g_p}}^2+r-1}{r}, \frac{\alpha_{g_p}}{r}, \ldots, \frac{\alpha_{g_p}+r-1}{r}, \frac{m_{g_p}}{r}, \ldots, \frac{m_{g_p}+r-1}{r}\right),$$
$$l_{h_2} = \left(\frac{{\xi_h}^2}{r}, \ldots, \frac{{\xi_h}^2+r-1}{r}, \frac{\alpha_h}{r}, \ldots, \frac{\alpha_h+r-1}{r}, \frac{m_h}{r}, \ldots, \frac{m_h+r-1}{r}\right).$$

D. CDF OF END-TO-END SNR FOR RIS-AIDED DUAL-HOP RF-FSO LINK

The CDF of γ_{eq} is expressed as

$$F_{\gamma_{eq}}(\gamma) = F_{\gamma_r}(\gamma) + F_{\gamma_d}(\gamma) - F_{\gamma_r}(\gamma) F_{\gamma_d}(\gamma). \quad (27)$$

Substituting (13) and (26) in (27) and carrying out algebraic calculations, the simplification of CDF of γ_{eq} can be attained as

$$F_{\gamma_{eq}}(\gamma) = \sum_{n=0}^{\infty} \frac{(-1)^n \left(\frac{1}{b_r\sqrt{\bar{\gamma}_r}}\right)^{a_r+1+n}}{n!\,(a_r+1+n)\,\Gamma(a_r+1)} + \frac{\xi_h^2 A_h \xi_{g_d}^2 A_{g_d}}{2^{2r}} \times \sum_{m_h=1}^{\beta_h} \sum_{m_{g_d}=1}^{\beta_{g_d}} b_{m_h} b_{m_{g_d}} \frac{r^{\alpha_h+\alpha_{g_d}+m_h+m_{g_d}-2}}{2\pi^{2(r-1)}} \times G_{2r+1,6r+1}^{6r,1}\left[\left(\frac{B_{hg_p}}{\gamma_2}\right)\gamma \middle| \begin{matrix} 1, l_{g_{d_1}}, l_{h_1} \\ l_{h_2}, l_{g_{d_2}}, 0 \end{matrix}\right] \times \left(1 - \sum_{n=0}^{\infty} \frac{(-1)^n \left(\frac{1}{b_r\sqrt{\bar{\gamma}_r}}\right)^{a_r+1+n}}{n!\,(a_r+1+n)\,\Gamma(a_r+1)}\right). \quad (28)$$

As per the comprehension discussed in the literature review section, the combination of RIS-assisted RF-FSO framework taking Rician and Málaga distributions into account has not yet been described in any current study within the literature. As a result, the expression found in (28) can be demonstrated to be unique. Also, the generalized depiction of both Rician and Málaga distribution drives this endeavor towards the goal of unifying the many existing models by treating them as prominent occurrences.

III. PERFORMANCE ANALYSIS

In this portion of the work, we attain the expressions for the suggested RIS-assisted RF-FSO network's metrics of performance, namely ASC, the lower bound of SOP, probability of SPSC, IP, and EST.

A. AVERAGE SECRECY CAPACITY ANALYSIS

ASC is the mean value of the instantaneous secrecy capacity, which can be stated analytically as [35], [40], and [64, Eq. (15)]

$$ASC^I = \int_0^{\infty} \frac{1}{1+\gamma} F_{\gamma_{e_p}}(\gamma) \left[1 - F_{\gamma_{eq}}(\gamma)\right] d\gamma. \quad (29)$$

On substituting (26) and (28) into (29), ASC is derived as

$$ASC^I = \mathcal{X}_1 \Bigg(\sum_{n=0}^{\infty} \mathcal{U}_1 - \sum_{n=0}^{\infty} \mathcal{X}_2 \mathcal{U}_2 - \sum_{m_h=1}^{\beta_h} \sum_{m_g=1}^{\beta_{g_d}} \mathcal{X}_3 \mathcal{U}_3 + \sum_{n=0}^{\infty} \sum_{m_h=1}^{\beta_h} \sum_{m_{g_d}=1}^{\beta_{g_d}} \mathcal{X}_2 \mathcal{X}_3 \mathcal{U}_4 \Bigg), \quad (30)$$

where

$$\mathcal{X}_1 = \frac{(-1)^n \left(\frac{1}{b_{e_p}\sqrt{\bar{\gamma}_r}}\right)^{a_{e_p}+n+1}}{n!\,(a_{e_p}+n+1)\,\Gamma(a_{e_p}+1)},$$
$$\mathcal{X}_2 = \frac{(-1)^n \left(\frac{1}{b_{e_p}\sqrt{\bar{\gamma}_r}}\right)^{a_r+n+1}}{n!\,(a_r+n+1)\,\Gamma(a_r+1)},$$
$$\mathcal{X}_3 = b_{m_h} b_{m_{g_d}} \frac{r^{\alpha_h+\alpha_{g_d}+m_h+m_{g_d}-2}}{2\pi^{2(r-1)}},$$

and four integral expressions $\mathcal{U}_1, \mathcal{U}_2, \mathcal{U}_3$ and $\mathcal{U}_4$ are expressed as follows.

1) DERIVATION OF $\mathcal{U}_1$

$\mathcal{U}_1$ is expressed as

$$\mathcal{U}_1 = \int_0^{\infty} \frac{\gamma^{\frac{a_{e_p}+n+1}{2}}}{1+\gamma} d\gamma. \quad (31)$$

With the fulfillment of identity [58, Eq. (3.194.3)], $\mathcal{U}_1$ is attained as

$$\mathcal{U}_1 = \mathcal{B}\left(\frac{a_{e_p}+n+3}{2}, 1 - \frac{a_{e_p}+n+3}{2}\right), \quad (32)$$

where $\mathcal{B}(.,.)$ is the Beta function [58, Eq. (8.39)].

2) DERIVATION OF $\mathcal{U}_2$

$\mathcal{U}_2$ is expressed as

$$\mathcal{U}_2 = \int_0^{\infty} \frac{\gamma^{\frac{a_r+a_{e_p}+2n+2}{2}}}{1+\gamma} d\gamma. \quad (33)$$

Using an analogous method to the one used to derive $\mathcal{U}_1, \mathcal{U}_2$ is closed in as

$$\mathcal{U}_2 = \mathcal{B}\left(\frac{a_r + a_{e_p} + 2n + 4}{2}, 1 - \frac{a_r + a_{e_p} + 2n + 4}{2}\right). \tag{34}$$

3) DERIVATION OF $\mathcal{U}_3$

$\mathcal{U}_3$ is expressed as

$$\mathcal{U}_3 = \int_0^\infty \frac{\gamma^{\frac{a_{e_p}+n+1}{2}}}{1+\gamma} G_{2r+1,6r+1}^{6r,1}\left[\left(\frac{B_{hg_p}}{\gamma_2}\right)\gamma \middle| \begin{matrix} 1, l_{d_1}, l_{h_1} \\ l_{h_2}, l_{d_2}, 0 \end{matrix}\right] d\gamma. \tag{35}$$

The transformation of $\frac{1}{1+\gamma}$ into Meijer's G function is done by utilizing the identity [62, Eq. (8.4.2.5)] and solving the integral upon utilization of [62, Eq. (2.24.1.1)], $\mathcal{U}_3$ is obtained as

$$\begin{aligned}\mathcal{U}_3 = &\int_0^\infty \gamma^{\frac{a_{e_p}+n+1}{2}} G_{2r+1,6r+1}^{6r,1}\left[\left(\frac{B_{hg_p}}{\gamma_2}\right)\gamma \middle| \begin{matrix} 1, l_{d_1}, l_{h_1} \\ l_{h_2}, l_{d_2}, 0 \end{matrix}\right] \\ &\times G_{1,1}^{1,1}\left[\gamma \middle| \begin{matrix} 0 \\ 0 \end{matrix}\right] d\gamma = \left(\frac{B_{hg_p}}{\gamma_2}\right)^{-\alpha_1} \\ &\times G_{6r+2,2r+2}^{2,6r+1}\left[\frac{\gamma_2}{B_{hg_p}} \middle| \begin{matrix} 0, -\alpha_1 - l_{h_2}, -\alpha_1 - l_{d_2}, -\alpha_1 \\ 0, -\alpha_1 - 1, -\alpha_1 - l_{d_1}, -\alpha_1 - l_{h_1} \end{matrix}\right],\end{aligned} \tag{36}$$

where $\alpha_1 = \frac{a_{e_p}+n+3}{2}$.

4) DERIVATION OF $\mathcal{U}_4$

$\mathcal{U}_4$ is expressed as

$$\begin{aligned}\mathcal{U}_4 = &\int_0^\infty \frac{1}{1+\gamma} \gamma^{\frac{a_r+a_{e_p}+2n+2}{2}} \\ &\times G_{2r+1,6r+1}^{6r,1}\left[\left(\frac{B_{hg_p}}{\bar{\gamma}_d}\right)\gamma \middle| \begin{matrix} 1, l_{d_1}, l_{h_1} \\ l_{h_2}, l_{d_2}, 0 \end{matrix}\right] d\gamma.\end{aligned} \tag{37}$$

Using an analogous method to the one used to derive $\mathcal{U}_3, \mathcal{U}_4$ is derived as

$$\begin{aligned}\mathcal{U}_4 = &\int_0^\infty \gamma^{\frac{a_{e_p}+n+1}{2}} G_{2r+1,6r+1}^{6r,1}\left[\left(\frac{B_{hg_p}}{\gamma_2}\right)\gamma \middle| \begin{matrix} 1, l_{d_1}, l_{h_1} \\ l_{h_2}, l_{d_2}, 0 \end{matrix}\right] \\ &\times G_{1,1}^{1,1}\left[\gamma \middle| \begin{matrix} 0 \\ 0 \end{matrix}\right] d\gamma = \left(\frac{B_{hg_p}}{\gamma_2}\right)^{-\alpha_2-1} \\ &\times G_{6r+2,2r+2}^{2,6r+1}\left[\frac{\gamma_2}{B_{hg_p}} \middle| \begin{matrix} 0, -\alpha_2 - l_{h_2}, -\alpha_2 - l_{d_2}, -\alpha_2 \\ 0, -\alpha_2 - 1, -\alpha_2 - l_{d_1}, -\alpha_2 - l_{h_1} \end{matrix}\right],\end{aligned} \tag{38}$$

where $\alpha_2 = \frac{a_r+a_{e_p}+2n+2}{2}$.

B. SECRECY OUTAGE PROBABILITY ANALYSIS

1) SCENARIO-I (LOWER BOUND SOP)

In accordance with [65, Eq. (21)], the lower bound of SOP can be stated as

$$SOP^I = \Pr\left\{\gamma_{eq} \le \phi\, \gamma_{\mathcal{E}}\right\} = \int_0^\infty F_{\gamma_{eq}}(\phi\,\gamma) f_{\gamma_{e_p}}(\gamma)\, d\gamma, \tag{39}$$

where $\phi = 2^{R_s}$ and R_s denotes the target secrecy rate. Now, substituting (12) and (28) into (39), SOP is expressed finally as

$$SOP^I = \frac{\mathcal{M}_1\mathcal{R}_1 + \mathcal{M}_2\mathcal{R}_2 - \mathcal{M}_3\mathcal{R}_3}{2b_{e_p}^{a_{e_p}+1}\Gamma(a_{e_p}+1)\bar{\gamma}_{e_p}^{\frac{a_{e_p}+1}{2}}}, \tag{40}$$

where

$$\mathcal{M}_1 = \sum_{n=0}^{\infty} \frac{(-1)^n}{n!\,(a_r+1+n)\,\Gamma(a_r+1)} \left(\frac{\phi^{\frac{1}{2}}}{b_r\sqrt{\bar{\gamma}_r}}\right)^{a_r+1+n},$$

$$\begin{aligned}\mathcal{M}_2 = &\frac{\xi_h^2 A_h \xi_{g_d}^2 A_{g_d}}{2^{2r}} \sum_{m_h=1}^{\beta_h}\sum_{m_{g_d}=1}^{\beta_{g_d}} b_{m_h} b_{m_{g_d}} \\ &\times \frac{r^{\alpha_h+\alpha_{g_d}+m_h+m_{g_d}-2}}{2\pi^{2(r-1)}},\end{aligned}$$

$$\begin{aligned}\mathcal{M}_3 = &\frac{\mathcal{M}_1 \xi_h^2 \xi_{g_d}^2}{2^{2r}} A_h A_{g_d} \sum_{m_h=1}^{\beta_h}\sum_{m_{g_d}=1}^{\beta_{g_d}} b_{m_h} b_{m_{g_d}} \\ &\times \frac{r^{\alpha_h+\alpha_{g_d}+m_h+m_{g_d}-2}}{2\pi^{2(r-1)}},\end{aligned}$$

and derivations of the three integral terms $\mathcal{R}_1, \mathcal{R}_2$ and $\mathcal{R}_3$ are expressed as follows.

2) DERIVATION OF $\mathcal{R}_1$

$\mathcal{R}_1$ is expressed as

$$\mathcal{R}_1 = \int_0^\infty \gamma^{\frac{a_r+a_{e_p}+n}{2}} e^{-\frac{\sqrt{\gamma}}{b_{e_p}\sqrt{\bar{\gamma}_{e_p}}}} d\gamma.$$

$\mathcal{R}_1$ is derived by utilizing [58, Eq. (3.326.2)] as

$$\mathcal{R}_1 = 2(a_r + a_{e_p} + n + 1)! \left(\frac{1}{b_{e_p}\sqrt{\bar{\gamma}_{e_p}}}\right)^{-a_r-a_{e_p}-n-2}. \tag{41}$$

3) DERIVATION OF $\mathcal{R}_2$

$\mathcal{R}_2$ is expressed as

$$\begin{aligned}\mathcal{R}_2 = &\int_0^\infty \gamma^{\frac{a_{e_p}+1}{2}-1} G_{2r+1,6r+1}^{6r,1}\left[\left(\frac{B_{hg_p}\phi}{\gamma_2}\right)\gamma \middle| \begin{matrix} 1, l_{d_1}, l_{h_1} \\ l_{h_2}, l_{d_2}, 0 \end{matrix}\right] \\ &\times e^{\frac{-\sqrt{\gamma}}{b_{e_p}\sqrt{\bar{\gamma}_{e_p}}}} d\gamma\end{aligned}$$

Now, through the use of a number of mathematical operations utilizing [62, Eq. (8.4.3.1) and (2.24.1.1)], $\mathcal{R}_2$ is derived as

$$\begin{aligned}\mathcal{R}_2 = &\int_0^\infty \gamma^{\frac{a_{e_p}+1}{2}-1} G_{2r+1,6r+1}^{6r,1}\left[\left(\frac{B_{hg_p}\phi}{\gamma_2}\right)\gamma \middle| \begin{matrix} 1, l_{d_1}, l_{h_1} \\ l_{h_2}, l_{d_2}, 0 \end{matrix}\right] \\ &\times G_{0,1}^{1,0}\left[\left(\frac{\sqrt{\gamma}}{b_{e_p}\sqrt{\bar{\gamma}_{e_p}}}\right) \middle| \begin{matrix} - \\ 0 \end{matrix}\right] d\gamma \\ = &\mathcal{Z}_1 G_{6r+1,2r+3}^{3,6r}\left[\frac{\gamma_2\left(\frac{1}{b_{e_p}\sqrt{\bar{\gamma}_{e_p}}}\right)^2}{4B_{hg_p}\phi} \middle| \begin{matrix} l_{h_3}, l_{d_3}, 1 - \frac{a_{e_p}+1}{2} \\ 0, -\frac{a_{e_p}+1}{2}, l_{d_4}, l_{h_4} \end{matrix}\right],\end{aligned} \tag{42}$$

where $\mathcal{Z}_1 = \pi^{-\frac{1}{2}} \left(\frac{\gamma_2}{B_{hg_p}\phi}\right)^{\frac{a_{ep}+1}{2}}$, $l_{h_3} = 1 - \frac{a_{ep}+1}{2} - l_{h_2}$, $l_{d_3} = 1 - \frac{a_{ep}+1}{2} - l_{d_2}$, $l_{h_4} = 1 - \frac{a_{ep}+1}{2} - l_{h_1}$, and $l_{d_4} = 1 - \frac{a_{ep}+1}{2} - l_{d_1}$.

4) DERIVATION OF $\mathcal{R}_3$

$\mathcal{R}_3$ is expressed as

$$\mathcal{R}_3 = \int_0^\infty \gamma^{\frac{a_r+a_{ep}+n}{2}} \mathrm{G}_{2r+1,6r+1}^{6r,1}\left[\left(\frac{B_{hg_p}\phi}{\gamma_2}\right)\gamma \middle| \begin{matrix} 1, l_{d_1}, l_{h_1} \\ l_{h_2}, l_{d_2}, 0 \end{matrix}\right] \times e^{\frac{-\sqrt{\gamma}}{b_{ep}\sqrt{\bar{\gamma}_{ep}}}} d\gamma.$$

Using an analogous method to the one used to derive $\mathcal{R}_2$, $\mathcal{R}_3$ is derived as

$$\begin{aligned}\mathcal{R}_3 &= \int_0^\infty \gamma^{\frac{a_r+a_{ep}+n}{2}} \mathrm{G}_{2r+1,6r+1}^{6r,1}\left[\left(\frac{B_{hg_p}\phi}{\gamma_2}\right)\gamma \middle| \begin{matrix} 1, l_{d_1}, l_{h_1} \\ l_{h_2}, l_{d_2}, 0 \end{matrix}\right] \\ &\quad \times \mathrm{G}_{0,1}^{1,0}\left[\left(\frac{\sqrt{\gamma}}{b_{e_p}\sqrt{\bar{\gamma}_{e_p}}}\right)\middle| \begin{matrix} - \\ 0 \end{matrix}\right] d\gamma \\ &= \mathcal{Z}_2 \mathrm{G}_{6r+1,2r+3}^{3,6r}\left[\frac{\left(\frac{1}{b_{e_p}\sqrt{\bar{\gamma}_{e_p}}}\right)^2}{4B_{hg_p}\phi}\gamma_2 \middle| \begin{matrix} l_{h_5}, l_{d_5}, 1-\mathcal{Z}_3 \\ 0, -\mathcal{Z}_3, l_{d_6}, l_{h_6} \end{matrix}\right],\end{aligned} \tag{43}$$

where $\mathcal{Z}_2 = \pi^{-\frac{1}{2}} \left(\frac{\gamma_2}{B_{hg_p}\phi}\right)^{\mathcal{Z}_3}$, $\mathcal{Z}_3 = \frac{a_r+a_{ep}+n+2}{2}$, $l_{h_5} = 1 - \mathcal{Z}_3 - l_{h_2}$, $l_{d_5} = 1 - \mathcal{Z}_3 - l_{d_2}$, $l_{h_6} = 1 - \mathcal{Z}_3 - l_{h_1}$, and $l_{d_6} = 1 - \mathcal{Z}_3 - l_{d_1}$.

5) SCENARIO-I (ASYMPTOTIC SOP)

For a better understanding of our analytical method in high SNR region, we derive asymptotic expressions of our lower bound SOP by assuming the condition $\gamma_2 \to \infty$. In general, the asymptotic expression of (40) is presented as

$$SOP^{I,\infty} = \frac{\mathcal{M}_1\mathcal{R}_1 + \mathcal{M}_2\mathcal{R}_4 - \mathcal{M}_3\mathcal{R}_5}{2b_{e_p}^{a_{ep}+1}\Gamma(a_{e_p}+1)\bar{\gamma}_{e_p}^{\frac{a_{ep}+1}{2}}}, \tag{44}$$

Here, $\mathcal{R}_4$ is formed by transforming the Meijer's G term in (42) via utilizing [60, Eq. (19)] as

$$\begin{aligned}\mathcal{R}_4 &= \mathcal{Z}_1 \sum_{y=1}^{6r} \Gamma(l_{d_{4,y}})\Gamma(l_{h_{4,y}})\left[\frac{\gamma_2\left(\frac{1}{b_{e_p}\sqrt{\bar{\gamma}_{e_p}}}\right)^2}{4B_{hg_p}\phi}\right]^{-l_{d_{4,y}}-l_{h_{4,y}}} \\ &\quad \times \frac{\prod_{\Theta=1,\Theta\neq y}^{6r}\Gamma(l_{d_{4,\Theta}}-l_{d_{4,y}})\Gamma(l_{h_{4,\Theta}}-l_{h_{4,y}})}{\prod_{\Theta=3}^{2r+3}\Gamma(l_{d_{3,\Theta}}-l_{d_{4,y}})\Gamma(l_{h_{3,\Theta}}-l_{h_{4,y}})}.\end{aligned} \tag{45}$$

Similarly, $\mathcal{R}_5$ is found from (43) as

$$\begin{aligned}\mathcal{R}_5 &= \mathcal{Z}_2 \sum_{y=1}^{6r} \Gamma(l_{d_{6,y}})\Gamma(l_{h_{6,y}})\left[\frac{\gamma_2\left(\frac{1}{b_{e_p}\sqrt{\bar{\gamma}_{e_p}}}\right)^2}{4B_{hg_p}\phi}\right]^{-l_{d_{6,y}}-l_{h_{6,y}}} \\ &\quad \times \frac{\prod_{\Theta=1,\Theta\neq y}^{6r}\Gamma(l_{d_{6,\Theta}}-l_{d_{6,y}})\Gamma(l_{h_{6,\Theta}}-l_{h_{6,y}})}{\prod_{\Theta=3}^{2r+3}\Gamma(l_{d_{5,\Theta}}-l_{d_{6,y}})\Gamma(l_{h_{5,\Theta}}-l_{h_{6,y}})}.\end{aligned} \tag{46}$$

6) SCENARIO-II (LOWER BOUND SOP)

The expression of SOP of RIS-aided combined RF-FSO channel when the eavesdropper is at the FSO link can be described as [11, Eq. (13)]

$$\begin{aligned}SOP^{II} &= \Pr\{C_{sc} \le R_s\} = \Pr\{\gamma_{eq} \le \phi\gamma\mathcal{E}_Q + \phi - 1\} \\ &= \int_0^\infty \int_{\phi\gamma+\phi-1}^\infty f_{\gamma_{eq}}(\gamma) f_{\gamma_{eq}}(\gamma)\, d\gamma_{eq} d\gamma \\ &= \int_0^\infty F_{\gamma_d}(\phi\gamma+\phi-1) f_{\gamma_{e_q}}(\gamma)\, d\gamma \\ &\quad \times (1 - F_{\gamma_d}(\phi-1)) + F_{\gamma_d}(\phi-1).\end{aligned} \tag{47}$$

where C_{sc} denotes the channel capacity for the $\mathcal{S}-\mathcal{R}-\mathcal{D}$ link. Due to mathematical process of obtaining the precise SOP closed-form formula being challenging, we deduce the mathematical expression of SOP at the lower-bound considering the variable gain relaying scheme as [11, Eq. (14)]

$$\begin{aligned}SOP^{II} \ge SOP^{L} &= \Pr\{\gamma_{eq} \le \phi\gamma_{e_p}\} \\ &= \int_0^\infty F_{\gamma_d}(\phi\gamma) f_{\gamma_{e_q}}(\gamma)\, d\gamma \\ &\quad \times (1 - F_{\gamma_d}(\phi-1)) + F_{\gamma_d}(\phi-1).\end{aligned} \tag{48}$$

Substituting Eqs. (24) and (26) into (48) and utilizing [62, Eq. (2.24.1.1)] yields

$$\begin{aligned}SOP^{II} &= \mathcal{S}_1 \sum_{m_h=1}^{\beta_h}\sum_{m_{g_d}=1}^{\beta_{g_d}}\sum_{m_{g_{eq}}=1}^{\beta_{g_{eq}}} \mathcal{S}_2 b_{m_h}^2 b_{m_{g_d}} b_{m_{g_{eq}}} \\ &\quad \times \mathrm{G}_{8r+1,8r+1}^{6r+1,6r}\left[\frac{\mathcal{B}_1\gamma_2}{\bar{\gamma}_{e_q}\phi}\middle| \begin{matrix} 1-l_{h_2}, 1-l_{d_2}, 1, l_{e_{q_1}}, l_{h_1} \\ l_{h_2}, l_{e_{q_2}}, 0, 1-l_{h_1}, 1-l_{d_1} \end{matrix}\right] \\ &\quad \times (1 - F_{\gamma_d}(\phi-1)) + F_{\gamma_d}(\phi-1),\end{aligned} \tag{49}$$

where

$$\begin{aligned}\mathcal{B}_1 &= \left(\frac{B_{g_{eq}}}{B_{g_d}}\right)^r, \\ \mathcal{S}_1 &= \frac{\xi_h^4 \xi_{g_d}^2 \xi_{g_{eq}}^2 A_h{}^2 A_{g_d} A_{g_{eq}}}{2^{2r}}, \\ \mathcal{S}_2 &= \frac{r^{2\alpha_h+\alpha_{g_d}+\alpha_{g_{eq}}+2m_h+m_{g_d}+m_{g_{eq}}-5}}{4\pi^{4(r-1)}}, \\ l_{e_{q_1}} &= \left(\frac{1+\xi_{g_{eq}}{}^2}{r}, \ldots, \frac{1+\xi_{g_{eq}}{}^2+r-1}{r}\right),\end{aligned}$$

$$l_{e_{q_2}} = \left(\frac{\xi_{g_{e_q}}{}^2}{r}, \ldots, \frac{\xi_{g_{e_q}}{}^2 + r - 1}{r}, \frac{\alpha_{g_{e_q}}}{r}, \ldots, \frac{\alpha_{g_{e_q}} + r - 1}{r}, \frac{m_{g_{e_q}}}{r}, \ldots, \frac{m_{g_{e_q}} + r - 1}{r} \right),$$

$$F_{\gamma_d}(\phi - 1) = \sum_{n=0}^{\infty} \frac{(-1)^n \left(\frac{1}{b_r \sqrt{\bar{\gamma}_r}} \right)^{a_r+n+1} (\phi - 1)^{\frac{a_r+n+1}{2}}}{n!\,(a_r + n + 1)}.$$

7) SCENARIO-II (ASYMPTOTIC SOP)

Applying some mathematical operations on the Meijer's G function in (49) by using [44, Eq. (29)], the asymptotic expression of lower bound SOP for *Scenario-II* is obtained as

$$SOP^{II,\infty} = \mathcal{S}_1 \sum_{m_h=1}^{\beta_h} \sum_{m_{g_d}=1}^{\beta_{g_d}} \sum_{m_{g_{eq}}=1}^{\beta_{g_{eq}}} \mathcal{S}_2 b_{m_h}^2 b_{m_{g_d}} b_{m_{g_{eq}}} \times \sum_{v=1}^{6r} \frac{\prod_{\iota=1,\iota\neq v}^{6r} \Gamma(\mathcal{V}_{1,v} - \mathcal{V}_{1,\iota})}{\prod_{\iota=6r+1}^{8r+1} \Gamma(1 + \mathcal{V}_{1,\iota} - \mathcal{V}_{1,v})} \times \frac{\prod_{\iota=1}^{6r+1} \Gamma(1 + \mathcal{V}_{2,\iota} - \mathcal{V}_{1,v})}{\prod_{\iota=6r+2}^{8r+1} \Gamma(\mathcal{V}_{1,v} - \mathcal{V}_{2,\iota})} \left[\frac{\mathcal{B}_1 \gamma_2}{\bar{\gamma}_{e_q} \phi} \right]^{\mathcal{V}_{1,v}-1}, \tag{50}$$

where $\mathcal{V}_1 = (1 - l_{h_2}, 1 - l_{d_2}, 1, l_{e_{q_1}}, l_{h_1})$ and $\mathcal{V}_2 = (l_{h_2}, l_{e_{q_2}}, 0, 1 - l_{h_1}, 1 - l_{d_1})$.

8) SCENARIO-III

The lower bound of SOP for RIS-aided mixed RF-FSO framework with simultaneous eavesdropping attack via the RF and FSO links can be defined as

$$SOP^{III} = 1 - (SOP_1 \times SOP_2), \tag{51}$$

where

$$SOP_1 = 1 - \int_0^{\infty} F_{\gamma_r}(\phi\gamma) f_{\gamma_{e_p}}(\gamma)\, d\gamma, \tag{52}$$

$$SOP_2 = 1 - \int_0^{\infty} F_{\gamma_d}(\phi\gamma) f_{\gamma_{e_q}}(\gamma)\, d\gamma. \tag{53}$$

By placing (12) and (13) into (52) and utilizing [58, Eq. (3.326.2)], SOP_1 is expressed as

$$SOP_1 = 1 - \frac{1}{b_{e_p}^{a_{e_p}+1} \bar{\gamma}_{e_p}^{\frac{a_{e_p}+1}{2}} \Gamma(a_{e_p} + 1)} \times \sum_{n=0}^{\infty} \frac{(-1)^n \left(\frac{\phi^{\frac{1}{2}}}{b_r \sqrt{\bar{\gamma}_r}} \right)^{a_r+1+n} \left(b_{e_p} \sqrt{\bar{\gamma}_{e_p}} \right)^{T_1} \Gamma(T_1)}{n!\,(a_r + n + 1)\,\Gamma(a_r + 1)}, \tag{54}$$

where $T_1 = (a_r + a_{e_p} + n + 2)$. Plugging (24) and (26) into (53), utilizing [62, Eq. (2.24.1.1)] to conduct integration and facilitating the expression, SOP_2 is obtained as

$$SOP_2 = 1 - \mathcal{S}_1 \sum_{m_h=1}^{\beta_h} \sum_{m_{g_d}=1}^{\beta_{g_d}} \sum_{m_{g_{eq}}=1}^{\beta_{g_{eq}}} \mathcal{S}_2 b_{m_h}^2 b_{m_{g_d}} b_{m_{g_{eq}}} \times \mathrm{G}_{8r+1,8r+1}^{6r+1,6r} \left[\mathcal{B}_1 \frac{\gamma_2}{\bar{\gamma}_{e_q} \phi} \middle| \begin{matrix} 1 - l_{h_2}, 1 - l_{d_2}, 1, l_{e_{q_1}}, l_{h_1} \\ l_{h_2}, l_{e_{q_2}}, 0, 1 - l_{h_1}, 1 - l_{d_1} \end{matrix} \right]. \tag{55}$$

C. STRICTLY POSITIVE SECRECY CAPACITY ANALYSIS

The probability of SPSC serves to be one of the critical performance metrics that assures a continuous data stream only when the secrecy capacity remains a positive value in order to maintain secrecy in optical wireless communication. Mathematically, probability of SPSC is characterized as [40, Eq. (25)]

$$SPSC = \Pr\{C_{sc} > 0\} = 1 - SOP|_{R_s=0}. \tag{56}$$

Formulation of probability of SPSC is readily obtained through substitution of the SOP formula from (40), (49), and (51) into (56). Hence,

$$SPSC^I = 1 - SOP^I|_{R_s=0}, \text{(Scenario-I)} \tag{57}$$

$$SPSC^{II} = 1 - SOP^{II}|_{R_s=0}, \text{(Scenario-II)} \tag{58}$$

$$SPSC^{III} = 1 - SOP^{III}|_{R_s=0}. \text{(Scenario-III)} \tag{59}$$

D. EFFECTIVE SECRECY THROUGHPUT (EST)

The EST is a gauge of performance indicator that clearly incorporates both tapping channel dependability and indemnity constraints. It essentially measures the mean rate at which secure data gets transmitted from the source to the destination with no interception. EST can be expressed numerically as [10, Eq. (5)]

$$EST = R_S(1 - SOP). \tag{60}$$

Formulation of EST is readily obtained through substitution of the SOP formula in (60). Hence,

$$EST^I = R_S(1 - SOP^I), \text{ (Scenario-I)} \tag{61}$$

$$EST^{II} = R_S(1 - SOP^{II}), \text{ (Scenario-II)} \tag{62}$$

$$EST^{III} = R_S(1 - SOP^{III}). \text{ (Scenario-III)} \tag{63}$$

E. INTERCEPT PROBABILITY (IP)

IP is another significant performance metric that offers additional insights into the secrecy performance of a communication system. It refers to the probability that an eavesdropper successfully intercepts the data maintained at the actual receiving device. In this situation, the eavesdropper's chances of successfully intercepting the legitimate message are notably high. Mathematically, it can be written as [66, Eq. (33)]

$$IP = \Pr\{C_{sc} < C_e\} = \Pr\{\gamma_{eq} < \gamma_{\mathcal{E}}\} = SOP|_{R_s=0}, \tag{64}$$

where C_e defines the channel capacity for the eavesdropper links. Similar to the probability of SPSC, IP can be demonstrated by substituting the analytical expressions of SOP from (40), (49), and (51) into (64). Hence,

$$IP^{I} = SOP^{I}|_{R_s=0}, \text{(Scenario-I)} \quad (65)$$

$$IP^{II} = SOP^{II}|_{R_s=0}, \text{(Scenario-II)} \quad (66)$$

$$IP^{III} = SOP^{III}|_{R_s=0}. \text{(Scenario-III)} \quad (67)$$

F. SIGNIFICANCE OF THE DERIVED EXPRESSIONS

In this study, the derived expressions for metrics such as ASC, SOP, SPSC, EST, and IP serve as quantitative indicators of the system's secrecy performance. These expressions not only validate the proposed theoretical framework's accuracy but also offer a deeper understanding of the relationships between secrecy metrics and system parameters. Through these expressions, it becomes evident how factors like fading characteristics, turbulence conditions, pointing errors, and attack scenarios impact the system's secrecy performance. This analysis facilitates insights into the system's ability to maintain secure communication, aiding its practical applicability. Additionally, the expressions provide valuable guidance for network designers, offering clear directions for design choices and optimization strategies.

IV. NUMERICAL RESULTS

In this section, we present some numerical results based on the deduced analytical expressions of secrecy performance indicators i.e. SOP, SPSC, IP, ASC, and EST. Our analytical results are demonstrated for all three eavesdropping scenarios. To corroborate those analytical outcomes, we also exhibit MC simulations via generating Rician and Málaga random variables in MATLAB. This simulation is performed by averaging 100,000 channel realizations to get each secrecy indicator value. Unless stated otherwise, all the analytical results are obtained by considering $K_1 = K_r = K_{e_p} = 2$, $\Omega_1 = \Omega_r = \Omega_{e_p} = 3$, $\alpha_h = \alpha_{g_d} = \alpha_{g_{e_q}} = 2.296$, $\beta_h = \beta_{g_d} = \beta_{g_{e_q}} = 2$, $\xi_h = \xi_{g_d} = \xi_{g_{e_q}} = 6.7$, $\mathcal{N}_1 = 2$, $\bar{\gamma}_r = \bar{\gamma}_d = 10$ dB, $\bar{\gamma}_{e_p} = \bar{\gamma}_{e_q} = -5$ dB, $R_s = 0.1$, $(\alpha, \beta) = (2.296, 2), (4.2, 3), (8, 4)$ for strong, moderate, and weak turbulence, and $r = 1$. Due to the rapid convergence of the infinite series, we opt to utilize only the initial 25 terms to compute the values of the secrecy metrics.

The impact of average SNR on EST performance for a selected range of target secrecy rate (R_s) is investigated in Figs. 2 and 3. Both outcomes are analyzed through a range of average SNR values for the RF main channel, denoted as $\bar{\gamma}_r$, ranging from -10 dB to 10 dB. In this context, Fig. 2 depicts *Scenario-I* (EST^I), while Fig. 3 corresponds to *Scenario-III* (EST^{III}). It is observed that both figures devise concave down-shaped curves where EST rises to a certain value of R_s then declines afterward. Several reasons are responsible for this event. A lower value of R_s requires fewer security maintenance resources, leading to increased EST. Furthermore, larger R_s exacerbates the channel condition by introducing additional noise, interference, and fading in the system that has a notable impact on EST. Supposedly, the EST vs R_s relation in Figs. 2 and 3 demonstrate the optimization between the secured transmission rate of the system and the required resources for maintaining security.

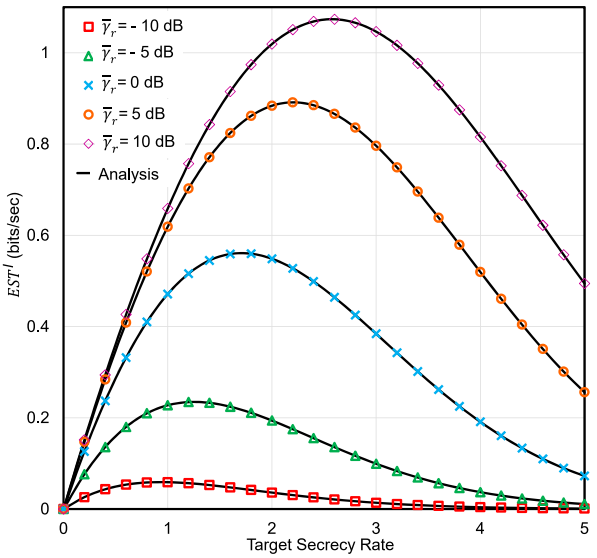

FIGURE 2. The EST^I versus R_s for selected values of $\bar{\gamma}_r$.

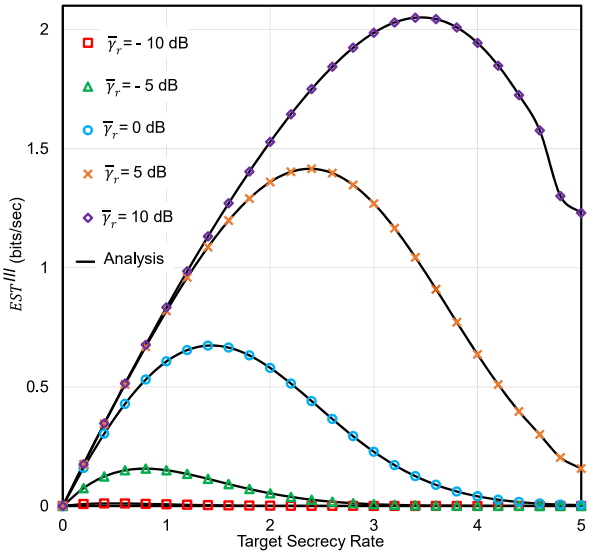

FIGURE 3. The EST^{III} versus R_s for selected values of $\bar{\gamma}_r$.

The impact of the shape parameter (K) and scale parameter (Ω) in Rician fading distribution on secrecy performance is investigated in Figs. 4 and 5. In Fig. 4, IP^I in *Scenario-I* decreases when Ω_1 and Ω_r from $\mathcal{S} - \mathcal{L}_{\mathcal{P}} - \mathcal{R}$ link are increased from 2 to 4, therefore, the secrecy performance improves. This behavior occurs because a higher scale parameter value improves signal quality by reducing signal attenuation, making the communication channel more reliable. For the same reason, secrecy performance downturns when Ω_{e_p} rises from 2 to 4 as it declines security of the main channel by strengthening $\mathcal{S} - \mathcal{L}_{\mathcal{P}} - \mathcal{E}_{\mathcal{P}}$ link. Additionally, the channel with a larger shape parameter experiences a lesser

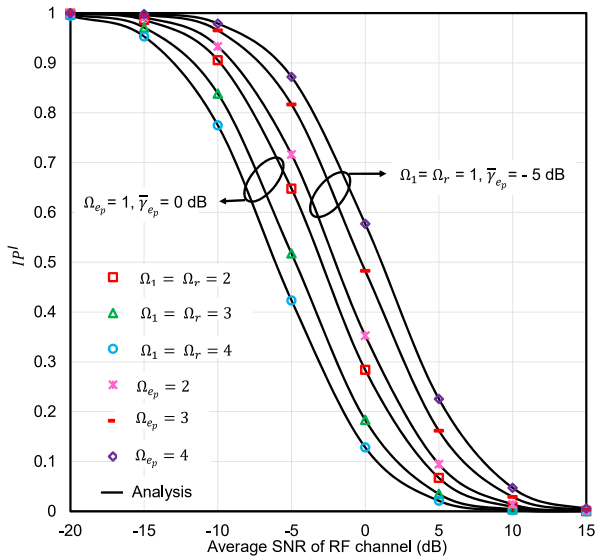

FIGURE 4. The IP^I versus $\bar{\gamma}_r$ for selected values of Ω_1, Ω_r, Ω_{ep}, and $\bar{\gamma}_{ep}$.

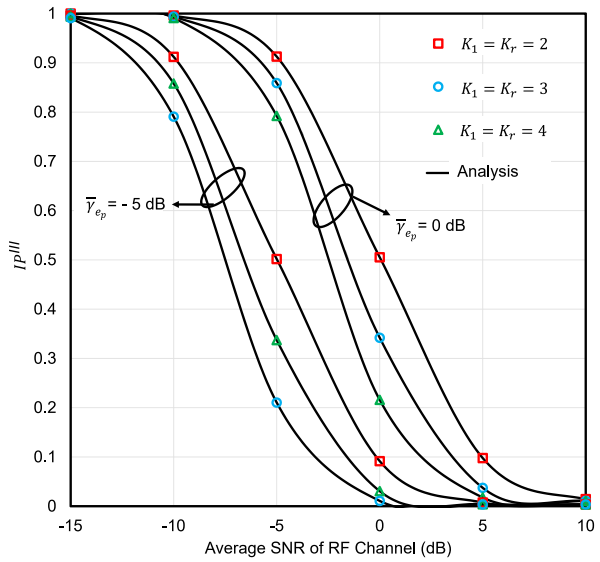

FIGURE 5. The IP^{III} versus $\bar{\gamma}_r$ for selected values of K_1, K_r, and $\bar{\gamma}_{ep}$.

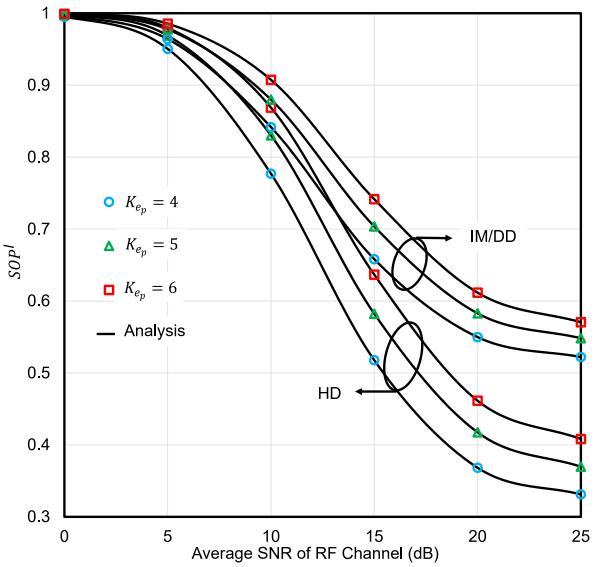

FIGURE 6. The SOP^I versus $\bar{\gamma}_r$ for selected values of K_{ep} and r.

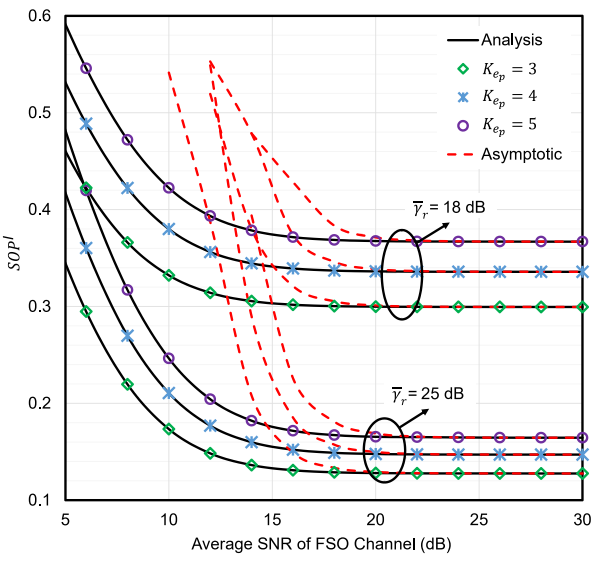

FIGURE 7. The SOP^I versus $\bar{\gamma}_d$ for selected values of K_{ep} and $\bar{\gamma}_r$.

fading effect. This is because the line-of-sight signal is much stronger than the scattered signal due to the higher value of K. This phenomenon is also justified in Fig. 5 for *Scenario-III* where system performance improves due to the higher values of K_1 and K_r. Furthermore, it can be concluded from both graphs that improved channel quality is attainable through larger Rician fading parameters and lower $\bar{\gamma}_{e_p}$.

Fig. 6 demonstrates a comparison between two detection techniques (i.e. HD and IM/DD) at the receiver for *Scenario-I*. Conventionally, the HD technique has the ability of frequency shifting in a high-frequency range. Thus, HD is less susceptible to wiretapping and contains more secrecy advantages than IM/DD for the secured wireless channel. Fig. 6 upholds this agreement and our analysis supports the results as testified in [40]. It can also be observed from Fig. 6 that a higher value of K_{e_p} lessens the fading effect of $\mathcal{S}-\mathcal{L}_{\mathcal{P}}-\mathcal{E}_{\mathcal{P}}$ link, thereby reinforcing wiretapping capability while diminishing overall system performance. The saturation of SOP at high SNR levels is readily apparent in the figure which is to be expected. The observed saturation phenomenon is primarily a result of the dominance of the weakest RF hop in this proposed RF-FSO configuration. Similar outcomes also observed in [41].

Fig. 7 shows the effect on SOP (*Scenario-I*) for different values of the SNR of $\mathcal{S}-\mathcal{L}_{\mathcal{P}}-\mathcal{R}$ link and shape parameter of $\mathcal{S}-\mathcal{L}_{\mathcal{P}}-\mathcal{E}_{\mathcal{P}}$ link, i.e., $\bar{\gamma}_r$ and K_{e_p}. Outcome shows that $\bar{\gamma}_r = 25$ dB exhibits better secrecy performance than $\bar{\gamma}_r = 18$ dB. However, system performance downturns while K_{e_p} is increasingly tuned from 3 to 5 in both SNR cases. Evidently, both higher $\bar{\gamma}_r$ and lower K_{e_p} not only increases

the strength of $\mathcal{S}-\mathcal{L}_{\mathcal{P}}-\mathcal{R}$ link but also lessens the impact of $\mathcal{S}-\mathcal{L}_{\mathcal{P}}-\mathcal{E}_{\mathcal{P}}$ link, hence lower SOP results. Moreover, the asymptotic expression explained in (44) is also implied in this figure, and result shows that asymptotic values match perfectly with analytical and simulation values in the higher SNR region.

The impact of FSO eavesdropper for *Scenario-II* is represented in both Figs. 8 and 9. It is observed that EST^{II} in Fig. 8 is higher for $\bar{\gamma}_{e_q} = 0$ dB compared to $\bar{\gamma}_{e_q} = 5$ dB. Moreover, SOP^{II} in Fig. 9 decreases when $\bar{\gamma}_{e_q}$ is tuned from 5 dB to -5 dB. These results are obvious as higher SNR of $\mathcal{R}-\mathcal{I}_{\mathcal{Q}}-\mathcal{E}_{\mathcal{Q}}$ link constantly increases the wiretapping capability of $\mathcal{E}_{\mathcal{Q}}$ that ultimately reduces the secrecy performance. It is also seen that the asymptotic results in Fig. 9 reveal exact match with the analytical results in higher $\bar{\gamma}_r$. This outcome is evident as both analytical and asymptotic results are theoretically bound to be equal while investigating the channel at high SNR region.

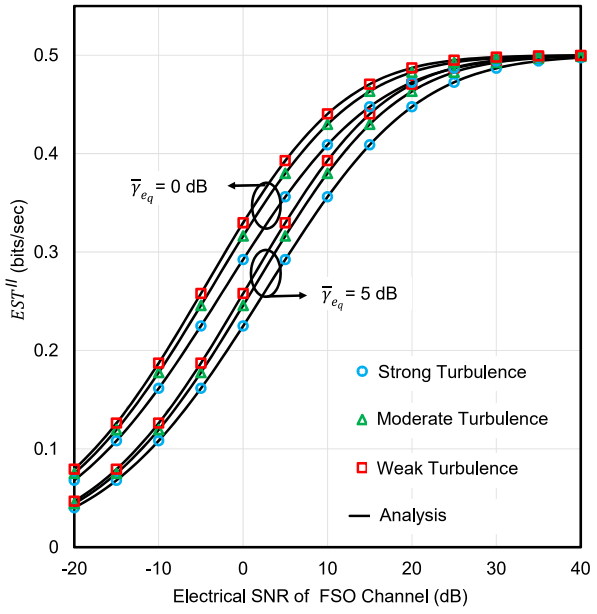

FIGURE 8. The EST^{II} versus $\bar{\gamma}_d$ for selected values of α_h, α_{g_d}, β_h, β_{g_d}, and $\bar{\gamma}_{e_q}$.

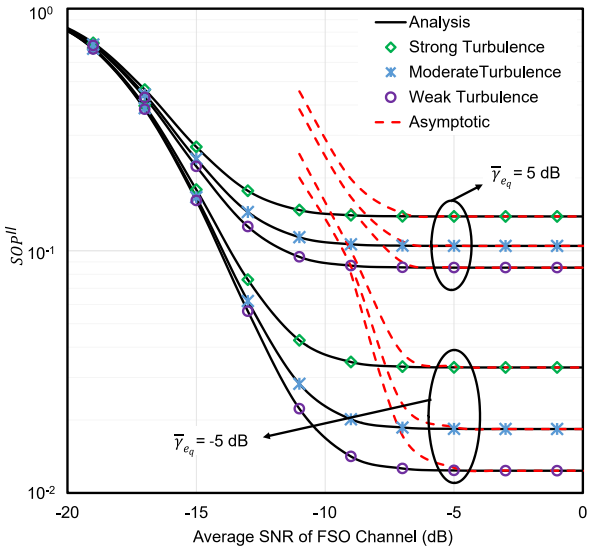

FIGURE 9. The SOP^{II} versus $\bar{\gamma}_d$ for selected values of α_h, α_{g_d}, β_h, β_{g_d}, and $\bar{\gamma}_{e_q}$.

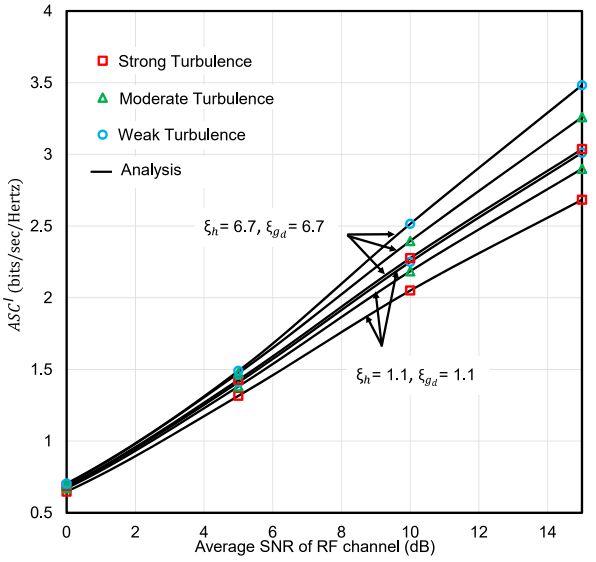

FIGURE 10. The ASC^I versus $\bar{\gamma}_r$ for selected values of α_h, α_{g_d}, β_h, β_{g_d}, ξ_h, and ξ_{g_d}.

The influence of the pointing error in the Málaga distribution on secrecy performance is studied in Figs. 10-12 due to all three scenarios. The findings clearly demonstrate that secrecy performance for three eavesdropping scenarios upturns when the pointing error index (ξ) increases from 1.1 (severe pointing error state) to 6.7 (negligible pointing error state). This outcome is consistent while varying both the average SNRs of the RF link (Figs. 10 and 12) and FSO link (Fig. 11). It is a notable fact that SOP^{III} in Fig. 12 downturns when $\mathcal{N}_1$ increases from 1 to 4. This occurrence serves as evidence that having a larger number of reflecting elements for the RIS-assisted fading model progressively enhances the system performance.

The effect of atmospheric turbulence conditions on EST, SOP, IP (*Scenario-II*), and ASC (*Scenario-I*) is investigated in Figs. 8-11. It can be observed that regardless of the different wiretapping scenarios, the secrecy performance of the proposed model improves when the turbulence condition of the FSO link shifts from strong turbulence to weak turbulence as demonstrated in [65]. This is due to the fact that the weak turbulence conditions allow for better control and compensation of atmospheric effects, leading to improved system performance in the FSO link compared to the more challenging conditions of severe turbulence.

A comparative analysis of *Scenario-I*, *Scenario-II* and *Scenario-III* for the proposed system model is presented in Fig. 13-14. In Fig. 13, the probability of SPSC is plotted

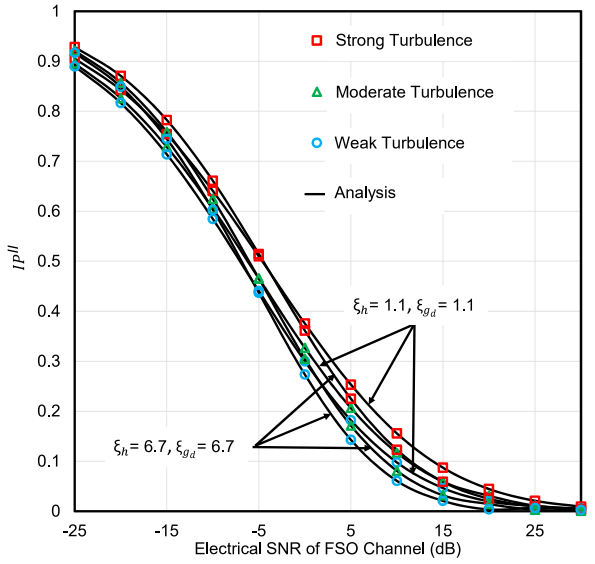

FIGURE 11. The IP^{II} versus $\bar{\gamma}_d$ for selected values of α_h, α_{g_d}, β_h, β_{g_d}, ξ_h, and ξ_{g_d}.

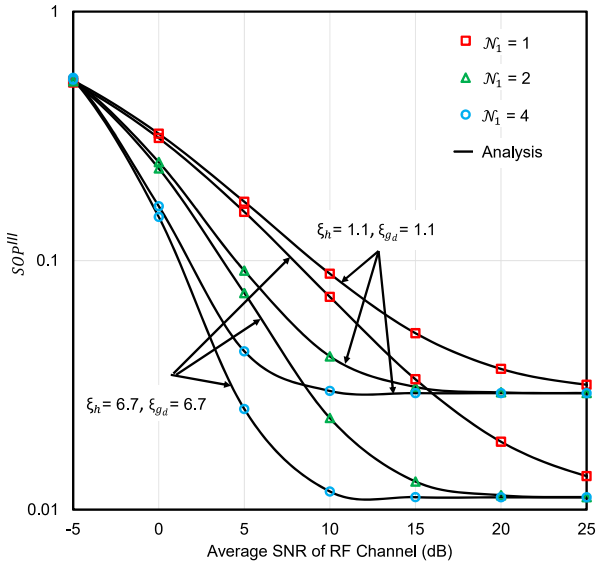

FIGURE 12. The SOP^{III} versus $\bar{\gamma}_r$ for selected values of $\mathcal{N}_1$, ξ_h and ξ_{g_d}.

against the average SNR of $\mathcal{R} - \mathcal{L}_\mathcal{Q} - \mathcal{D}$ link, i.e., γ_2 utilizing the derived expressions of (57)-(59). Conventionally, an FSO link is more secure and has lower susceptibility to eavesdropping compared to the RF link [41]. This can be proved also from Fig. 14. From the figure, it is seen that SOP for *Scenario-I* is higher than *Scenario-II*. Our analysis confirms the validity of this statement. Likewise, *Scenario-I* is worse than *Scenario-II* since the RF link is usually more vulnerable to wiretapping than the FSO link. However, from the Fig. 13, it is seen that the worst case is displayed by $SPSC^{III}$ (*Scenario-III*). The reason behind this case is both $\mathcal{E}_\mathcal{P}$ and $\mathcal{E}_\mathcal{Q}$ remain active simultaneously in *Scenario-III* that eventually creates the strongest form of eavesdropping for the channel.

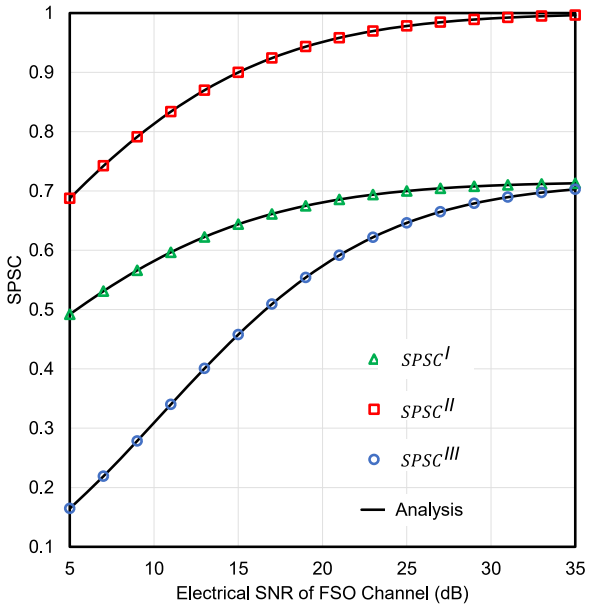

FIGURE 13. The *SPSC* versus $\bar{\gamma}_d$ for different eavesdropping scenarios.

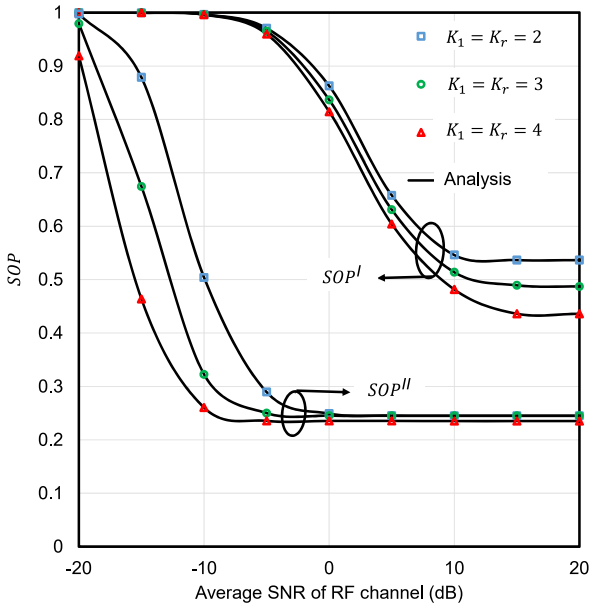

FIGURE 14. The *SOP* versus $\bar{\gamma}_r$ for different eavesdropping scenarios.

A. DESIGN GUIDELINES

In this section, some important guidelines that can be utilized in the design of practical RF-FSO mixed systems are provided.

- Fig. 12 demonstrates the notable performance enhancement achieved by incorporating RIS in both RF and FSO links, affirming their valuable contribution to the practical design of a RF-FSO mixed model.
- Given the modeling of the FSO link with a Málaga-distributed turbulent channel, employing the HD technique at the receiver side offers a superior estimation

approach for RF-FSO systems, effectively mitigating turbulence-induced fading while maintaining a high SNR.

- The impact of pointing error is pivotal in RF-FSO mixed systems, as demonstrated in Fig. 11. To mitigate this effect, it is advisable to employ larger diameter transmitters and receivers [67].

V. CONCLUSION

This study aimed at analyzing the security performance of a DF-based RIS-aided RF-FSO communication system in the presence of wiretapping attacks in both RF and FSO networks. We derived closed-form expressions for various performance metrics, such as ASC, EST, IP, probability of SPSC, and lower-bound SOP, to efficiently evaluate the impact of each parameter on the secrecy performance. The study validated its analytical outcomes using MC simulations. Numerical results reveal that fading severity, pointing errors, and natural turbulence parameters have a significant impact on secrecy performance. The study also explores the trade-off between the target secrecy rate and the resources required to maintain security via EST. Moreover, the result highlights the superiority of HD over IM/DD for optical signal detection. We also conducted a comparative analysis of three proposed wiretapping scenarios and concluded that simultaneous wiretapping has a more detrimental effect on the secrecy performance than individual wiretapping. Finally, it is claimed that the FSO link is less susceptible to wiretapping than the RF link.

REFERENCES

[1] M. Di Renzo, A. Zappone, M. Debbah, M.-S. Alouini, C. Yuen, J. de Rosny, and S. Tretyakov, "Smart radio environments empowered by reconfigurable intelligent surfaces: How it works, state of research, and the road ahead," *IEEE J. Sel. Areas Commun.*, vol. 38, no. 11, pp. 2450–2525, Nov. 2020.

[2] M. Shahjalal, W. Kim, W. Khalid, S. Moon, M. Khan, S. Liu, S. Lim, E. Kim, D.-W. Yun, J. Lee, W.-C. Lee, S.-H. Hwang, D. Kim, J.-W. Lee, H. Yu, Y. Sung, and Y. M. Jang, "Enabling technologies for AI empowered 6G massive radio access networks," *ICT Exp.*, vol. 9, no. 3, pp. 341–355, Jun. 2023.

[3] S. Noh, J. Lee, G. Lee, K. Seo, Y. Sung, and H. Yu, "Channel estimation techniques for RIS-assisted communication: Millimeter-wave and sub-THz systems," *IEEE Veh. Technol. Mag.*, vol. 17, no. 2, pp. 64–73, Jun. 2022.

[4] W. Khalid, Z. Kaleem, R. Ullah, T. V. Chien, S. Noh, and H. Yu, "Simultaneous transmitting and reflecting-reconfigurable intelligent surface in 6G: Design guidelines and future perspectives," *IEEE Netw.*, early access, Dec. 12, 2022, doi: 10.1109/MNET.129.2200389.

[5] H. Yu, H. Lee, and H. Jeon, "What is 5G? Emerging 5G mobile services and network requirements," *Sustainability*, vol. 9, no. 10, p. 1848, Oct. 2017.

[6] L. Yang, J. Yang, W. Xie, M. O. Hasna, T. Tsiftsis, and M. D. Renzo, "Secrecy performance analysis of RIS-aided wireless communication systems," *IEEE Trans. Veh. Technol.*, vol. 69, no. 10, pp. 12296–12300, Oct. 2020.

[7] T. N. Do, G. Kaddoum, T. L. Nguyen, D. B. da Costa, and Z. J. Haas, "Multi-RIS-aided wireless systems: Statistical characterization and performance analysis," *IEEE Trans. Commun.*, vol. 69, no. 12, pp. 8641–8658, Dec. 2021.

[8] E. Soleimani-Nasab and M. Uysal, "Generalized performance analysis of mixed RF/FSO cooperative systems," *IEEE Trans. Wireless Commun.*, vol. 15, no. 1, pp. 714–727, Jan. 2016.

[9] M. Ibrahim, A. S. M. Badrudduza, M. S. Hossen, M. K. Kundu, I. S. Ansari, and I. Ahmed, "On effective secrecy throughput of underlay spectrum sharing $\alpha-\mu$/Málaga hybrid model under interference-and-transmit power constraints," *IEEE Photon. J.*, vol. 15, no. 2, pp. 1–13, Apr. 2023.

[10] H. Lei, H. Luo, K.-H. Park, I. S. Ansari, W. Lei, G. Pan, and M.-S. Alouini, "On secure mixed RF-FSO systems with TAS and imperfect CSI," *IEEE Trans. Commun.*, vol. 68, no. 7, pp. 4461–4475, Jul. 2020.

[11] N. A. Sarker, A. Badrudduza, S. R. Islam, S. H. Islam, M. K. Kundu, I. S. Ansari, and K.-S. Kwak, "On the intercept probability and secure outage analysis of mixed (α-κ-μ)-shadowed and Málaga turbulent models," *IEEE Access*, vol. 9, pp. 133849–133860, 2021.

[12] E. Zedini, H. Soury, and M.-S. Alouini, "On the performance analysis of dual-hop mixed FSO/RF systems," *IEEE Trans. Wireless Commun.*, vol. 15, no. 5, pp. 3679–3689, May 2016.

[13] L. Yang, M. O. Hasna, and I. S. Ansari, "Unified performance analysis for multiuser mixed μ-η and $\mathcal{M}$-distribution dual-hop RF/FSO systems," *IEEE Trans. Commun.*, vol. 65, no. 8, pp. 3601–3613, Aug. 2017.

[14] L. Qu, G. Xu, Z. Zeng, N. Zhang, and Q. Zhang, "UAV-assisted RF/FSO relay system for space-air-ground integrated network: A performance analysis," *IEEE Trans. Wireless Commun.*, vol. 21, no. 8, pp. 6211–6225, Aug. 2022.

[15] B. Ashrafzadeh, E. Soleimani-Nasab, M. Kamandar, and M. Uysal, "A framework on the performance analysis of dual-hop mixed FSO-RF cooperative systems," *IEEE Trans. Commun.*, vol. 67, no. 7, pp. 4939–4954, Jul. 2019.

[16] I. S. Ansari, M. M. Abdallah, M.-S. Alouini, and K. A. Qaraqe, "A performance study of two hop transmission in mixed underlay RF and FSO fading channels," in *Proc. IEEE Wireless Commun. Netw. Conf. (WCNC)*, Apr. 2014, pp. 388–393.

[17] I. S. Ansari, F. Yilmaz, and M.-S. Alouini, "On the performance of hybrid RF and RF/FSO dual-hop transmission systems," in *Proc. 2nd Int. Workshop Opt. Wireless Commun. (IWOW)*, Oct. 2013, pp. 45–49.

[18] Y. Zhang, J. Zhang, M. D. Renzo, H. Xiao, and B. Ai, "Performance analysis of RIS-aided systems with practical phase shift and amplitude response," *IEEE Trans. Veh. Technol.*, vol. 70, no. 5, pp. 4501–4511, May 2021.

[19] D. Selimis, K. P. Peppas, G. C. Alexandropoulos, and F. I. Lazarakis, "On the performance analysis of RIS-empowered communications over Nakagami-*m* fading," *IEEE Commun. Lett.*, vol. 25, no. 7, pp. 2191–2195, Jul. 2021.

[20] P. Xu, W. Niu, G. Chen, Y. Li, and Y. Li, "Performance analysis of RIS-assisted systems with statistical channel state information," *IEEE Trans. Veh. Technol.*, vol. 71, no. 1, pp. 1089–1094, Jan. 2022.

[21] B. Al-Nahhas, M. Obeed, A. Chaaban, and M. J. Hossain, "RIS-aided cell-free massive MIMO: Performance analysis and competitiveness," in *Proc. IEEE Int. Conf. Commun. Workshops (ICC Workshops)*, Jun. 2021, pp. 1–6.

[22] M. R. A. Ruku, M. Ibrahim, A. S. M. Badrudduza, and I. S. Ansari, "Effects of co-channel interference on RIS empowered wireless networks amid multiple eavesdropping attempts," 2023, *arXiv:2302.10876*.

[23] R. A. Tasci, F. Kilinc, E. Basar, and G. C. Alexandropoulos, "A new RIS architecture with a single power amplifier: Energy efficiency and error performance analysis," *IEEE Access*, vol. 10, pp. 44804–44815, 2022.

[24] P. Yang, L. Yang, and S. Wang, "Performance analysis for RIS-aided wireless systems with imperfect CSI," *IEEE Wireless Commun. Lett.*, vol. 11, no. 3, pp. 588–592, Mar. 2022.

[25] A. M. Salhab and L. Yang, "Mixed RF/FSO relay networks: RIS-equipped RF source vs RIS-aided RF source," *IEEE Wireless Commun. Lett.*, vol. 10, no. 8, pp. 1712–1716, Aug. 2021.

[26] L. Yang, W. Guo, and I. S. Ansari, "Mixed dual-hop FSO-RF communication systems through reconfigurable intelligent surface," *IEEE Commun. Lett.*, vol. 24, no. 7, pp. 1558–1562, Jul. 2020.

[27] A. Sikri, A. Mathur, P. Saxena, M. R. Bhatnagar, and G. Kaddoum, "Reconfigurable intelligent surface for mixed FSO-RF systems with co-channel interference," *IEEE Commun. Lett.*, vol. 25, no. 5, pp. 1605–1609, May 2021.

[28] L. Yang, F. Meng, J. Zhang, M. O. Hasna, and M. D. Renzo, "On the performance of RIS-assisted dual-hop UAV communication systems," *IEEE Trans. Veh. Technol.*, vol. 69, no. 9, pp. 10385–10390, Sep. 2020.

[29] S. Malik, P. Saxena, and Y. H. Chung, "Performance analysis of a UAV-based IRS-assisted hybrid RF/FSO link with pointing and phase shift errors," *J. Opt. Commun. Netw.*, vol. 14, no. 4, pp. 303–315, Apr. 2022.

[30] G. D. Verma, A. Mathur, Y. Ai, and M. Cheffena, "Mixed dual-hop IRS-assisted FSO-RF communication system with H-ARQ protocols," *IEEE Commun. Lett.*, vol. 26, no. 2, pp. 384–388, Feb. 2022.

[31] A. S. M. Badrudduza, M. Ibrahim, S. M. R. Islam, M. S. Hossen, M. K. Kundu, I. S. Ansari, and H. Yu, "Security at the physical layer over GG fading and mEGG turbulence induced RF-UOWC mixed system," *IEEE Access*, vol. 9, pp. 18123–18136, 2021.

[32] J. Zhang, T. Duong, R. Woods, and A. Marshall, "Securing wireless communications of the Internet of Things from the physical layer, an overview," *Entropy*, vol. 19, no. 8, p. 420, Aug. 2017.

[33] M. Ibrahim, M. Z. I. Sarkar, A. S. M. Badrudduza, M. K. Kundu, and S. Dev, "Impact of correlation on the security in multicasting through k–μ shadowed fading channels," in *Proc. IEEE Region 10 Symp. (TENSYMP)*, Jun. 2020, pp. 1396–1399.

[34] H. Yu and J. Joung, "Secure IoT communications using HARQ-based beamforming for MISOSE channels," *IEEE Internet Things J.*, vol. 8, no. 23, pp. 17211–17226, Dec. 2021.

[35] H. Yu, T. Kim, and H. Jafarkhani, "Wireless secure communication with beamforming and jamming in time-varying wiretap channels," *IEEE Trans. Inf. Forensics Security*, vol. 13, no. 8, pp. 2087–2100, Aug. 2018.

[36] H. Yu and J. Joung, "Design of the power and dimension of artificial noise for secure communication systems," *IEEE Trans. Commun.*, vol. 69, no. 6, pp. 4001–4010, Jun. 2021.

[37] H. Yu and T. Kim, "Training and data structures for AN-aided secure communication," *IEEE Syst. J.*, vol. 13, no. 3, pp. 2869–2872, Sep. 2019.

[38] H. Yu and I.-G. Lee, "Physical layer security based on NOMA and AJ for MISOSE channels with an untrusted relay," *Future Gener. Comput. Syst.*, vol. 102, pp. 611–618, Jan. 2020.

[39] E. Erdogan, I. Altunbas, G. K. Kurt, and H. Yanikomeroglu, "The secrecy comparison of RF and FSO eavesdropping attacks in mixed RF-FSO relay networks," *IEEE Photon. J.*, vol. 14, no. 1, pp. 1–8, Feb. 2022.

[40] S. H. Islam, A. S. M. Badrudduza, S. M. Riazul Islam, F. I. Shahid, I. S. Ansari, M. K. Kundu, S. K. Ghosh, M. B. Hossain, A. S. M. S. Hosen, and G. H. Cho, "On secrecy performance of mixed generalized gamma and Málaga RF-FSO variable gain relaying channel," *IEEE Access*, vol. 8, pp. 104127–104138, 2020.

[41] N. A. Sarker, A. S. M. Badrudduza, M. K. Kundu, and I. S. Ansari, "Effects of eavesdropper on the performance of mixed $\eta-\mu$ and DGG cooperative relaying system," 2021, *arXiv:2106.06951*.

[42] D. R. Pattanayak, V. K. Dwivedi, V. Karwal, A. Upadhya, H. Lei, and G. Singh, "Secure transmission for energy efficient parallel mixed FSO/RF system in presence of independent eavesdroppers," *IEEE Photon. J.*, vol. 14, no. 1, pp. 1–14, Feb. 2022.

[43] Y. Ai, A. Mathur, H. Lei, M. Cheffena, and I. S. Ansari, "Secrecy enhancement of RF backhaul system with parallel FSO communication link," *Opt. Commun.*, vol. 475, Nov. 2020, Art. no. 126193.

[44] D. R. Pattanayak, V. K. Dwivedi, V. Karwal, I. S. Ansari, H. Lei, and M.-S. Alouini, "On the physical layer security of a decode and forward based mixed FSO/RF co-operative system," *IEEE Wireless Commun. Lett.*, vol. 9, no. 7, pp. 1031–1035, Jul. 2020.

[45] Y. Wang, Y. Tong, and Z. Zhan, "On secrecy performance of mixed RF-FSO systems with a wireless-powered friendly jammer," *IEEE Photon. J.*, vol. 14, no. 2, pp. 1–8, Apr. 2022.

[46] M. J. Saber and S. Rajabi, "On secrecy performance of millimeter-wave RF-assisted FSO communication systems," *IEEE Syst. J.*, vol. 15, no. 3, pp. 3781–3788, Sep. 2021.

[47] S. H. Islam, A. Badrudduza, S. R. Islam, F. I. Shahid, I. S. Ansari, M. K. Kundu, and H. Yu, "Impact of correlation and pointing error on secure outage performance over arbitrary correlated Nakagami-*m* and $\mathcal{M}$-turbulent fading mixed RF-FSO channel," *IEEE Photon. J.*, vol. 13, no. 2, pp. 1–17, Apr. 2021.

[48] L. Wei, K. Wang, C. Pan, and M. Elkashlan, "Secrecy performance analysis of RIS-aided communication system with randomly flying eavesdroppers," *IEEE Wireless Commun. Lett.*, vol. 11, no. 10, pp. 2240–2244, Oct. 2022.

[49] A. K. Yadav, S. Yadav, A. Pandey, and A. Silva, "On the secrecy performance of RIS-enabled wireless communications over Nakagami-*m* fading channels," *ICT Exp.*, vol. 9, no. 3, pp. 452–458, Jun. 2023.

[50] X. Zhao and J. Sun, "Secure reconfigurable intelligent surface aided heterogeneous VLC-RF cooperative NOMA networks," *Opt. Commun.*, vol. 511, May 2022, Art. no. 127983.

[51] D. Wang, M. Wu, Z. Wei, K. Yu, L. Min, and S. Mumtaz, "Uplink secrecy performance of RIS-based RF/FSO three-dimension heterogeneous networks," *IEEE Trans. Wireless Commun.*, early access, Jul. 12, 2023, doi: 10.1109/TWC.2023.3292073.

[52] W. Khalid, H. Yu, D.-T. Do, Z. Kaleem, and S. Noh, "RIS-aided physical layer security with full-duplex jamming in underlay D2D networks," *IEEE Access*, vol. 9, pp. 99667–99679, 2021.

[53] A. M. Salhab and M. H. Samuh, "Accurate performance analysis of reconfigurable intelligent surfaces over Rician fading channels," *IEEE Wireless Commun. Lett.*, vol. 10, no. 5, pp. 1051–1055, May 2021.

[54] M. K. Ghosh, M. K. Kundu, M. Ibrahim, A. S. M. Badrudduza, M. S. Anower, I. S. Ansari, A. A. Shaikhi, and M. A. Mohandes, "Secrecy outage analysis of energy harvesting relay-based mixed UOWC-RF network with multiple eavesdroppers," 2023, *arXiv:2302.10257*.

[55] X. Pan, H. Ran, G. Pan, Y. Xie, and J. Zhang, "On secrecy analysis of DF based dual hop mixed RF-FSO systems," *IEEE Access*, vol. 7, pp. 66725–66730, 2019.

[56] Q. Chen, M. Li, X. Yang, R. Alturki, M. D. Alshehri, and F. Khan, "Impact of residual hardware impairment on the IoT secrecy performance of RIS-assisted NOMA networks," *IEEE Access*, vol. 9, pp. 42583–42592, 2021.

[57] Y. Xu, J. Xia, H. Wu, and L. Fan, "Q-learning based physical-layer secure game against multiagent attacks," *IEEE Access*, vol. 7, pp. 49212–49222, 2019.

[58] I. Gradshteyn, I. Ryzhik, and R. H. Romer, "Tables of integrals, series, and products," *Amer. Inst. Phys.*, vol. 56, no. 10, p. 958, Oct. 1988.

[59] A. R. Ndjiongue, T. M. N. Ngatched, O. A. Dobre, A. G. Armada, and H. Haas, "Analysis of RIS-based terrestrial-FSO link over G-G turbulence with distance and jitter ratios," *J. Lightw. Technol.*, vol. 39, no. 21, pp. 6746–6758, Nov. 1, 2021.

[60] I. S. Ansari, F. Yilmaz, and M.-S. Alouini, "Performance analysis of free-space optical links over Málaga ($\mathcal{M}$) turbulence channels with pointing errors," *IEEE Trans. Wireless Commun.*, vol. 15, no. 1, pp. 91–102, Jan. 2016.

[61] D. Karp and E. Prilepkina, "Hypergeometric differential equation and new identities for the coefficients of Nørlund and bühring," *Symmetry, Integrability Geometry, Methods Appl.*, vol. 12, p. 52, May 2016.

[62] Y. A. Brychkov, O. Marichev, and A. Prudnikov, *Integrals and Series, Volume 3: More Special Functions*. Amsterdam, The Netherlands: Gordon Breach Science, 1986.

[63] *Mathematica Edition: Version 8.0*, Wolfram Research, Champaign, IL, USA, 2010.

[64] W. Khalid, H. Yu, R. Ali, and R. Ullah, "Advanced physical-layer technologies for beyond 5G wireless communication networks," *Sensors*, vol. 21, no. 9, p. 3197, May 2021.

[65] N. A. Sarker, A. S. M. Badrudduza, S. M. R. Islam, S. H. Islam, I. S. Ansari, M. K. Kundu, Mst. F. Samad, M. B. Hossain, and H. Yu, "Secrecy performance analysis of mixed hyper-Gamma and Gamma-Gamma cooperative relaying system," *IEEE Access*, vol. 8, pp. 131273–131285, 2020.

[66] E. Illi, F. El Bouanani, D. B. Da Costa, F. Ayoub, and U. S. Dias, "Dual-hop mixed RF-UOW communication system: A PHY security analysis," *IEEE Access*, vol. 6, pp. 55345–55360, 2018.

[67] E. Erdogan, N. Kabaoglu, I. Altunbas, and H. Yanikomeroglu, "On the error probability of cognitive RF-FSO relay networks over Rayleigh/EW fading channels with primary-secondary interference," *IEEE Photon. J.*, vol. 12, no. 1, pp. 1–13, Feb. 2020.

MD. MIJANUR RAHMAN is currently pursuing the B.Sc. degree in electronics and telecommunication engineering (ETE) with the Rajshahi University of Engineering and Technology (RUET), Rajshahi, Bangladesh. His current research interests include FSO communication and physical layer security.

A. S. M. BADRUDDUZA (Member, IEEE) received the B.Sc. and M.Sc. degrees in electrical and electronic engineering (EEE) from the Rajshahi University of Engineering and Technology (RUET), Rajshahi, Bangladesh, in 2016 and 2019, respectively. From September 2016 to July 2017, he was a Lecturer with the Department of EEE, Bangladesh Army University of Engineering and Technology (BAUET), Natore, Rajshahi. From July 2017 to June 2020, he was a Lecturer with the Department of Electronics and Telecommunication Engineering (ETE), RUET, where he has been an Assistant Professor, since June 2020. He has authored/coauthored more than 40 international journals/conference publications. His current research interests include physical layer security in multicast, cellular and cooperative networks, free space optics (FSO), underwater optics (UWO), and NOMA systems.

Mr. Badrudduza was a recipient of two EEE Association Awards (Student of the Year Award) from RUET for his outstanding academic performances in the first and fourth-year examinations while pursuing the B.Sc.Eng. degree and the three best paper awards for three different research papers from the IEEE Region 10 Symposium (TENSYMP2020), the Third IEEE International Conference on Telecommunication and Photonics (ICTP2019), and the International Conference on Electrical, Computer and Communication Engineering (ECCE 2023). He has been affiliated with IEEE, since 2020, and is an active reviewer of several IEEE journals.

NOOR AHMAD SARKER received the B.Sc. degree in electronics and telecommunication engineering (ETE) from the Rajshahi University of Engineering and Technology (RUET), Rajshahi, Bangladesh. His current research interests include physical layer security, cooperative communication, RIS technology, and FSO communication.

MD. IBRAHIM (Graduate Student Member, IEEE) received the B.Sc. degree in electrical and electronic engineering (EEE) from the Rajshahi University of Engineering and Technology (RUET), Rajshahi, Bangladesh, in 2021. From September 2021 to December 2021, he was a Lecturer with the Department of EEE, Varendra University (VU), Rajshahi. He has been a Lecturer with the Institute of Information and Communication Technology (ICT), RUET, since December 2021. His current research interests include free-space optics communication, physical layer security, underwater communications, cognitive radio networks, and NOMA systems. He has been affiliated with IEEE, since 2022, and is an active reviewer of several IEEE journals.

IMRAN SHAFIQUE ANSARI (Senior Member, IEEE) received the B.Sc. degree (Hons.) in computer engineering from the King Fahd University of Petroleum and Minerals (KFUPM), in 2009, and the M.Sc. and Ph.D. degrees from the King Abdullah University of Science and Technology (KAUST), in 2010 and 2015, respectively.

Since August 2018, he has been a Lecturer (an Assistant Professor) with the University of Glasgow, Glasgow, U.K. Prior to this, he was a Lecturer (an Assistant Professor) with the Global College of Engineering and Technology (GCET), from November 2017 to July 2018 (affiliated with the University of the West of England (UWE), Bristol, U.K.) From April 2015 to November 2017, he was a Postdoctoral Research Associate (PRA) with Texas A&M University at Qatar (TAMUQ). From May 2009 to August 2009, he was a Visiting Scholar with Michigan State University (MSU), East Lansing, MI, USA. From June 2010 to August 2010, he was a Research Intern with Carleton University, Ottawa, ON, Canada. He has authored/coauthored more than 100 journals and conference publications. His current research interests include free-space optics (FSO), underwater communications, physical layer secrecy issues, full duplex systems, and secure D2D applications for 5G+ systems.

Dr. Ansari has been affiliated with IEEE and IET, since 2007, and has served in various capacities. He has served as a TPC member for various IEEE conferences. He has co-organized the GRASNET, in 2016, 2017, and 2018, workshops in conjunction with IEEE WCNC, in 2016 and 2017, and IEEE Globecom, in 2018. He was a recipient of an Exemplary Reviewer for IEEE TRANSACTION ON COMMUNICATIONS, in 2018 and 2016, and IEEE WIRELESS COMMUNICATIONS LETTERS, in 2017 and 2014. He was a recipient of the TAMUQ ECEN Research Excellence Award, in 2016 and 2017, the Reviewer Certificate by *Optics Communications* (Elsevier), in 2015, the Reviewer Certificate by OSA Publishing, in 2014, the Postdoctoral Research Award (PDRA) (First Cycle) with Qatar National Research Foundation (QNRF), in 2014, the KAUST Academic Excellence Award (AEA), in 2014, and the IEEE Richard E. Merwin Student Scholarship Award, in July 2013. He served on the IEEE Nominations and Appointments (N&A) Committee, from 2020 to 2021, and the IEEE Communication Society Young Professionals (ComSoc YP) Board, since April 2016. He has been a part of the IEEE 5G Tech Focus Publications Editorial Board, since February 2017. He is serving as the Past-Chair for the IET Young Professionals Communities Committee (YPCC), from October 2020 to September 2021. He has served on the IET Satellites Technical Network (TN), from March 2016 to September 2020. He has served on the IET Communities Committee-Europe, Middle-East and Africa (CC-EMEA), for two complete terms, from October 2015 to September 2018 and October 2010 to September 2013. He is an active reviewer for various IEEE TRANSACTIONS and various other journals.

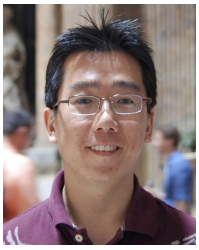

HEEJUNG YU (Senior Member, IEEE) received the B.S. degree in radio science and engineering from Korea University, Seoul, South Korea, in 1999, and the M.S. and Ph.D. degrees in electrical engineering from the Korea Advanced Institute of Science and Technology (KAIST), Daejeon, South Korea, in 2001 and 2011, respectively. From 2001 to 2012, he was with the Electronics and Telecommunications Research Institute (ETRI), Daejeon. From 2012 to 2019, he was with Yeungman University, South Korea. Currently, he is a Professor with the Department of Electronics and Information Engineering, Korea University, Sejong, South Korea. His current research interests include statistical signal processing and communication theory.